Geol. Mag. **147** (*4*), *2010, pp. 551–569. © Cambridge University Press 2010*
doi:10.1017/S0016756809990628

Geochronology and structural relationships of mesothermal gold mineralization in the Palaeoproterozoic Jokisivu prospect, southern Finland

K. SAALMANN*†, I. MÄNTTÄRI*, P. PELTONEN*, M. J. WHITEHOUSE‡, P. GRÖNHOLM§ & M. TALIKKA§

*Geological Survey of Finland, P.O. Box 96, FI-02151 Espoo, Finland
‡Laboratory for Isotope Geology, Swedish Museum of Natural History, P.O. Box 50 007, SE-104 05 Stockholm, Sweden
§Polar Mining Oy, Kummunkatu 34, 83500 Outokumpu, Finland

(*Received* 23 April 2009; *accepted* 31 July 2009; First published online 18 January 2010)

Abstract – The palaeoproterozoic Svecofennian orogen in southern Finland contains a number of orogenic gold occurrences. The Jokisivu gold deposit, comprising auriferous quartz veins, is hosted by syn-tectonic quartz diorites to gabbros. Mineralization occurs in approximately WNW–ESE- and WSW–ENE-trending shear zones, which probably branch from regional-scale NW–SE-trending shears. Ore zone fabrics post-date regional-scale folding and the metamorphic peak, and can be correlated with late Svecofennian regional shear tectonics (D_6; 1.83–1.78 Ga), indicating that mineralization formed during the late stages of orogenic evolution. SIMS and TIMS U–Pb dating of three samples place tight constraints on the age of gold mineralization. Zircons from both unaltered and altered quartz diorites have ages of 1884 ± 4 Ma and 1881 ± 3 Ma, respectively. These are interpreted as the crystallization age of the rock and as providing the maximum age for mineralization. Zircon rims from an altered quartz diorite from the ore zone give ages of *c*. 1802 ± 15 Ma, which overlap with the 1801 ± 18 Ma titanite (mean Pb–Pb) age from the ore zone. The ages are similar to the age of the pegmatite dyke that cuts the ore zone and whose zircon age of 1807 ± 3 Ma is approximately the same as the 1791 ± 2 Ma monazite age (TIMS) giving the minimum age of the gold mineralization. The mineralization and its structural framework can be correlated with coeval late Svecofennian shear tectonics related to WNW–ESE-oriented shortening in southern Finland. Extensive *c*. 1.8 Ga granite magmatism, shear zone development and associated gold mineralization are of regional importance also in the northern and western Fennoscandian Shield (Finnish Lapand and Sweden). A Cordilleran-type setting can explain the widespread distribution of magmatism and gold mineralization associated with shortening, as well as the required heat source triggering hydrothermal fluid flow along shear zones.

Keywords: U–Pb geochronology, orogenic gold, structural geology, Svecofennian orogeny, tectonic model, Finland.

1. Introduction

The Palaeoproterozoic Svecofennian orogen in Finland contains a number of gold occurrences of various genetic types; many of these could be classified as orogenic gold linked to shear zones (Eilu *et al.* 2003). Some prospects have been studied in detail; however, these studies were mostly restricted to the prospect-scale without considering links to the regional-scale structures and the tectonic evolution. The age of gold mineralization in southern Finland is also poorly known, hampering a regional interpretation and correlation of metallogenic provinces and events. In the light of a complex and polyphase tectonic evolution of the Svecofennian domain, the determination of the age of mineralized shear zones is critical for understanding the origin and tectonic setting of regional mineralization episodes as well as their genetic relationships.

The Jokisivu prospect lies in southern Finland (Fig. 1), in the border zone between the Pirkanmaa belt and the Häme belt. These belts are considered to belong to two crustal blocks that were amalgamated during the Svecofennian orogeny (e.g. Lahtinen, Korja & Nironen, 2005). The deposit has been classified as orogenic (Eilu, 2007), and is under feasibility study and test mining by Polar Mining Oy/Dragon Mining NL. The gold is hosted by a quartz diorite to gabbro (referred to as quartz diorite in the following text). Mineralization is controlled by shear zones which cut the quartz diorite.

Structural observations, data collection and sampling for this study have been carried out mainly in two opened trenches and a small test pit in the prospect area. The major aim of this study is to date the mineralization event and to link it with the structural and tectonic evolution of this area.

1.a. Geological setting

The Svecofennian Orogen in southern Finland has been divided into (1) a primitive arc complex west of the

†Author for correspondence: kerstin.saalmann@gtk.fi

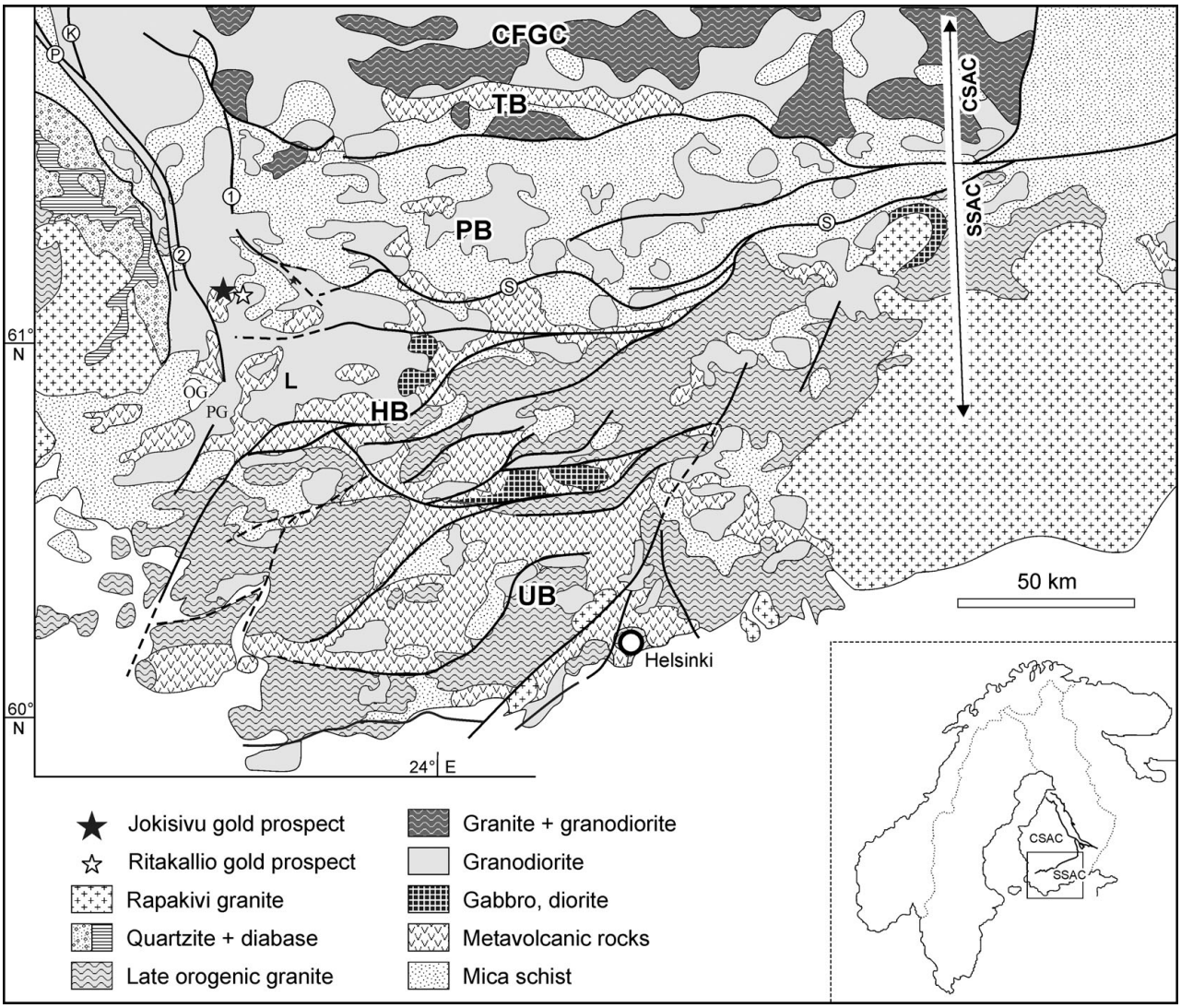

Figure 1. Geological map of southern Finland (after Korsman *et al.* 1997, modified and supplemented) with location of the Jokisivu prospect. CFGC – Central Finland granitoid complex; TB – Tampere schist belt; PB – Pirkanmaa belt; HB – Häme schist belt; UB – Uusimaa belt; L – Loimaa area; PG – Pöytyä granodiorite; OG – Oripää granite; numbered sheared zones: 1– Kankaanpää shear zone; 2 – Pori/Kynsikangas shear zone: P – continuation of the Pori shear zone; K – continuation of the Kynsikangas shear zone; S – suture proposed by Lahtinen (1994); SSAC – Southern Svecofennian Arc Complex; CSAC – Central Svecofennian Arc Complex.

archaean Karelian craton, (2) the Central Svecofennian Arc Complex, and (3) the Southern Svecofennian Arc Complex (Korsman *et al.* 1997) (Fig. 1).

The Central Svecofennian Arc Complex contains the Central Finland Granitoid Complex, the volcano-sedimentary Tampere schist belt, the Pohjanmaa belt and the Pirkanmaa belt consisting mainly of migmatitic turbidites.

The Southern Svecofennian Arc Complex containing the Häme and Uusimaa belts is characterized by a strong overprint by late Svecofennian orogenic events between 1.84 and 1.79 Ga. The Häme belt consists of *c.* 1.89–1.88 Ga calc-alkaline arc-type volcanic rocks intercalated with minor metasedimentary units (Hakkarainen, 1994; Kähkönen, Lahtinen & Nironen, 1994). The Uusima belt comprises remnants of 1.91–1.88 Ga island-arc-related magmatic and metaedimentary rocks (Huhma, 1986; Patchett & Kouvo, 1986; Väisänen, Mänttäri & Hölttä, 2002). A characteristic feature is a 100 km, ~W–E-trending high temperature–low pressure amphibolite- to granulite-facies migmatite zone with *c.* 1.84–1.82 Ga S-type granites (Korsman *et al.* 1999). The Southern Svecofennian Arc Complex could be traced to the southwest to Bergslagen in Sweden, containing similar arc-type rocks (Valbracht, Oen & Beunk, 1994; Allen *et al.* 1996).

Isotope-geochemical data and zircon geochronology suggest the presence of *c.* 2.0 Ga evolved thick continental crust under the Central Finland Granitoid Complex (Kähkönen, Huhma & Aro, 1989; Nironen & Kähkönen, 1994; Lahtinen & Huhma, 1997; Rämö *et al.* 2001), called the Keitele microcontinent by Lahtinen, Korja & Nironen (2005). Two billion year old continental crust is inferred to underlie the Häme and Uusimaa belts as well, but is suggested by Lahtinen, Korja & Nironen (2005) to belong to another microcontinent (Bergslagen microcontinent).

https://doi.org/10.1017/S0016756809990628 Published online by Cambridge University Press

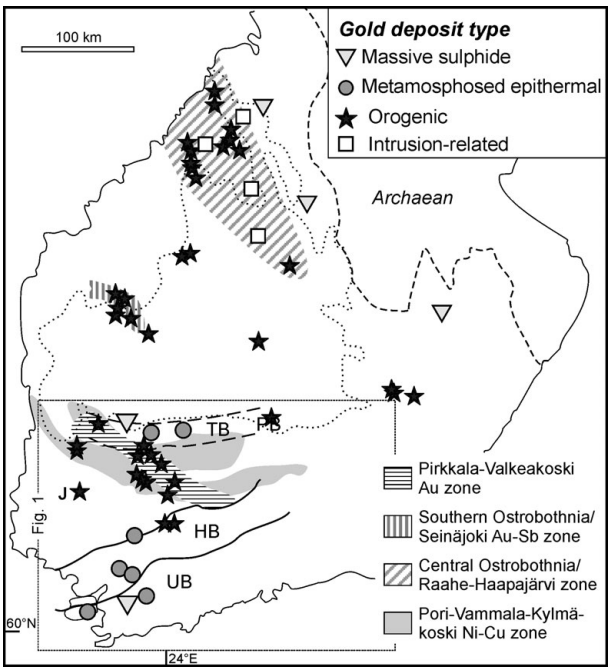

Figure 2. Gold occurrences and mineralization styles in southern Finland (source: Saltikoff, Puustinen & Tontti, 2006; Eilu, 2007). TB – Tampere schist belt; PB – Pirkanmaa belt; HB – Häme schist belt; UB – Uusimaa belt. J – Jokisivu prospect. Box outlines – map area in Figure 1.

The suture zone between these two continental blocks is proposed to be located in the southern Pirkanmaa belt (Lahtinen, 1994, 1996) (Fig. 1).

The (post-1.92 Ga) tectono-metamorphic history of the southern Svecofennian domain can be divided into two major cycles, each comprising a HT metamorphic event (e.g. Korsman *et al.* 1999): an early Svecofennian cycle at *c.* 1.91–1.86 Ga, and a late Svecofennian cycle at *c.* 1.84–1.80 Ga, separated by an extensional episode between *c.* 1.86 and 1.84 Ga.

2. Geology of the Jokisivu area

The Jokisivu prospect lies at 61.11739N, 22.62019E in the border zone between the southwestern Pirkanmaa belt and the Häme belt (Fig. 1). The distinction between these units, and their boundary, is not well defined, however, it is important since it marks the supposed suture zone between the Central Svecofennian and Southern Svecofennian Arc complexes. The geology of the region is characterized by a complex interplay of several generations of interfering folds and shear zones, and it may include several thrust sheets. Although the location of the boundary between the Häme and Pirkanmaa belts is far from resolved, the Jokisivu prospect is usually regarded as being part of the Pirkanmaa belt (Eilu, 2007; Saltikoff, Puustinen & Tontti, 2006). This region is recognized for its Ni–Cu potential (Puustinen, Saltikoff & Tontti, 1995) (Fig. 2). The Pirkkala–Valkeakoski Au zone of Saltikoff, Puustinen & Tontti (2006) (Fig. 2) overlaps with the Ni–Cu zone and comprises several minor gold mineralizations. The Jokisivu prospect and other small occurrences are located south of this zone, and Saltikoff, Puustinen & Tontti (2006) speculate whether they may form a separate province.

2.a. Lithological units

The bedrock of the Jokisivu area is composed of granodioritic to tonalitic gneisses, mica gneisses and minor mafic to intermediate volcanic rocks. The mica gneisses are migmatitic with tonalitic to trondhjemitic leucosomes and quartzo-feldspatic veins and pods. Some leucosome patches are granitic in composition and apparently represent later intrusions.

The mica gneisses are intercalated with metavolcanites and granodioritic and tonalitic gneisses. The supracrustal units are intruded by gabbroic to quartz-dioritic rocks.

Plutonic to subvolcanic gabbroic to quartz dioritic rocks intruding nearly concordantly into the pre-existing mica gneiss succession occur in the Pirkanmaa belt (Matisto, 1978; Kilpeläinen, 1998; Rutland, Williams & Korsman, 2004) and in the Loimaa area (Häme belt) (Nironen, 1999). The Jokisivu gold deposit is hosted by such an intrusion that hosts two ore zones (see Section 2.c). Large parts of the medium-grained rock look homogeneous; however, both grain size and hornblende content may locally vary over short distances, leading to a patchy appearance of the rock. Locally it also displays a layered fabric. The quartz diorite contains elongated mafic enclaves and displays a strong alignment of hornblende and plagioclase.

Granites occur to the southwest of the study area. Some are medium-grained but the majority are pegmatitic and they contain gneissic and metavolcanic xenoliths of the country rocks (Luukkonen, 1994).

Numerous pegmatite dykes truncate the succession; they occur also in the Jokisivu deposit (see Section 2.b.4). It is not clear whether at least some of these pegmatitic dykes may belong to the granites or if they form a distinct event.

2.b. Structural evolution

Geological and aeromagnetic maps (Fig. 3) illustrate a complex geometry resulting from polyphase deformation. The Jokisivu prospect is located in an area with interference of three stages of folding (F_3, F_4, F_5), followed by later shearing. This multiple-stage history with overprinting folds, foliations and lineations often make it impossible to assess the foliation–lineation relationships with certainty in this region. An overview of the structural evolution and correlation with the Loimaa area (Häme belt) and Pirkanmaa belt is presented in Figure 4.

The compositional layering within the mica gneisses in the Jokisivu area represents a composite foliation that transposed earlier layering or banding. In a few cases, intimate small-scale isoclinal folding may be recognized. In similar supracrustal rocks of the Loima

https://doi.org/10.1017/S0016756809990628 Published online by Cambridge University Press

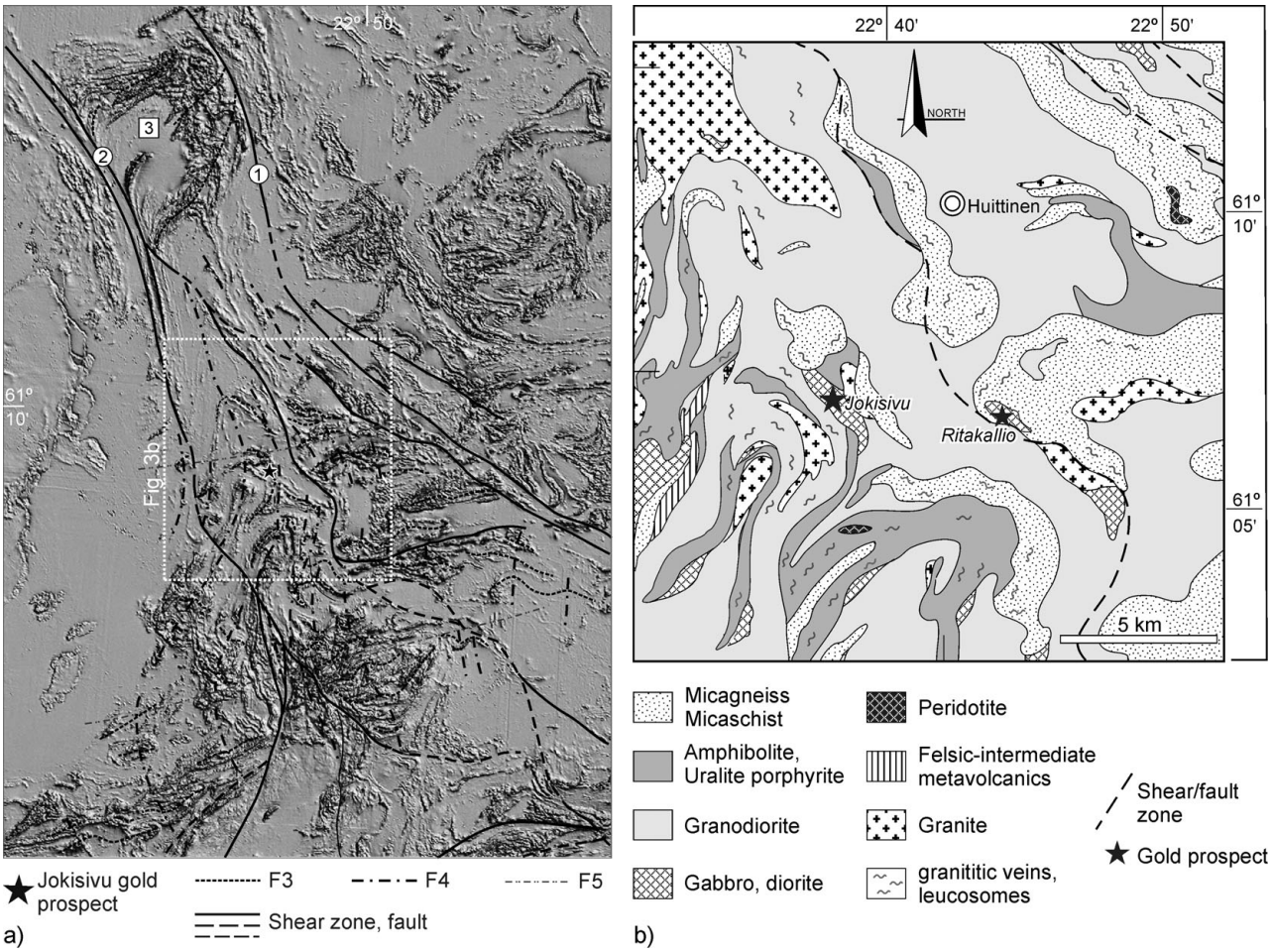

Figure 3. (a) Aeromagnetic map of the Jokisivu area illustrating different fold generations and major shear zones. The Jokisivu prospect is located in the outer hinge of a NE–SW-trending F_4 fold. In this area, F_4 fold axes curve from a SW–NE trend to a NW–SE trend caused by open F_5 and drag along major NW–SE-trending shear zones. 1 – Kankaanpää shear zone; 2 – Pori/Kynsikangas shear zone; 3 – Pomarkku block. Box outlines the area in (b). (b) Geological map of the Jokisivu area (after Matisto, 1978). Location of the Jokisivu deposit as well as the Ritakallio prospect showing comparable structures and mineralization.

area, an older internal foliation S_1 is preserved in porphyroblasts surrounded by the external foliation S_2 (Nironen, 1999). Thus, for comparison, the compositional layering in the Jokisivu area is also labelled $S_{1–2}$.

2.b.1. D_3

Prominent structures on the maps are regional-scale tight to isoclinal folds with subvertical axial planes that formed during D_3. Emplacement of the quartz diorite hosting the gold mineralization at Jokisivu occurred either prior to, or in the early stages of, F_3 folding. Because of the tight to isoclinal F_3 fold shape, S_3 and the F_3 axial planes are nearly parallel to $S_{1–2}$ in the mica schists. The original F_3 trend was probably approximately WSW–ENE to E–W. In the Jokisivu area, F_3 fold axial planes strike NW–SE because of later deformation (Figs 3, 4). Migmatitic leucosome veins in the mica gneisses cutting the layering $S_{1–2}$ at a low angle have been folded together with the layering. Leucosome veins also occur parallel to F_3 fold axial planes and in the fold hinge zones. The observed migmatitic structures correspond well to D_3 features in migmatitic mica schists of the Loima area south of the study area described by Nironen (1999), supporting the interpretation of syn-D_3 migmatization.

2.b.2. D_4, D_5

Tight F_4 folds with sub-horizontal fold axes and steep to sub-vertical fold axial planes cause F_3/F_4 regional dome and basin interference patterns (Fig. 3). On outcrop-scale, F_4 is represented by crenulation and chevron-like folds that are second or third order folds to the map-scale F_4 structures. S_4 is a crenulation cleavage. The Jokisivu deposit is located in the outer hinge zone of a NE–SW-trending regional-scale F_4 fold that refolds earlier F_3 folds (Fig. 3). In the Jokisivu prospect the crenulation lineation L_4 and F_4 fold axes plunge to the NE. Further northwest and south, the F_4 axial plane trend changes to NNW–SSE directions. This curvature is caused by F_5 open folding (Figs 3, 4), as well as by drag along major NW–SE-trending, late tectonic shear zones (D_6, see next Section).

https://doi.org/10.1017/S0016756809990628 Published online by Cambridge University Press

Jokisivu area (this paper)		Loimaa area (Nironen, 1999)	Pirkanmaa belt (Kilpeläinen, 1998)	Approx. age	
S_1 in metasedimentary rocks	D_1	microfolded inclusion trails in K-feldspar porphyroblasts	D_1 horizontal S_1 parallel S_0 migmatisation (1890-1885 Ma)		
S_{0-2} composite foliation, metamorphism (mica gneiss, mica schists)	D_2	S_{0-2} composite foliation, metamorphism			
intrusion of quartz diorite		syn-D_2 intrusion of tonalite granodiorite	intrusion of quartz diorite	**1882 ± 4 Ma**	
F_3 tight to isoclinal folds, E-W trending steep fold axial planes; migmatization, leucosomes; shearing (parallel to F_3 limbs)	D_3	F_3 tight to isoclinal folds, E-W trending steep fold axial planes; migmatization, leucosomes; shearing	F_2 isoclinal folds, D_2 E-W steep axial planes; migmatisation (1889-1878 Ma)	1.88-1.86 Ga *1880 ± 6 Ma*[3] *1878*[2]*,1875*[1] *Ma*	*early Svecofennian cycle*
		Pöytyä granodiorite		1.87[4] Ga	
F_4 open to tight folds, NNW-SSE trending steep fold axial planes, F3-F4 dome and basin patterns, folding ore zone; ?pegmatitic leucosome veins?	D_4	Oripää granite F4 open to tight folds, N-S steep axial planes dome and basin patterns	D_3 conjugate folds, vertical fold axial planes 1) SW-NE, dex 2) NW-SE, sini high-strain zones with S3; local migmatization in D3 high-strain zones	< *1872±10 Ma / 1850±16 Ma*[5]	
F_5 open folding/flexuring ~WSW-ENE trending axes	D_5				
~ESE-WNE and ENE-WSW trending shear zones with early pegmatite dikes and quartz veins gold mineralization	D_6	E-W shear zones			*late Svecofennian cycle*
pegmatite intrusion				**1801 ± 18 Ma** **1807 ± 3 Ma**	
late stage SW-NE dextral faults with rusty quartz veins	post-D_6			< 1.80 Ga	
top-NW directed oblique reverse slip on SW-NE striking faults; en echelon quartz veins; $\sigma1$~NW-SE	Faults with SW-directed sinistral oblique reverse slip (reactivation of pre-existing NNE- to NE-dipping foliation planes) $\sigma1$~SW-NE			< 1.79 Ga	

[1]Monazite (Hopgood et al. 1983); [2]Monazite (Mouri, Korsman & Huhma, 1999), [3]Monazite Rutland, Williams & Korsman, 2004);
[4]Pöytyä granodiorite (Nironen 1999), [5]Oripää granite (Kurhila et al. 2005) - probably inherited zircon grains; **bold**: obtained ages in this study

Figure 4. Correlation of the structural evolution in the Jokisivu area with the Loimaa area (Häme belt; Nironen, 1999) and the Pirkanmaa belt (Kilpeläinen, 1998). An estimation of the age of deformation is given based on structural correlation, the obtained analyses and data from the literature.

2.b.3. D_6 shearing

Major NW–SE (mainly NE-dipping)- and ~E–W-trending shear and fault zones (D_6) cut the dome and basin fold structures (Figs 1, 3).

NW–SE to WNW–ESE-trending shear zones cutting the quartz diorite in the Jokisivu prospect (Fig. 5) play a major role in gold mineralization. The shear zone in the Kujankallio ore zone splays into NW–SE- and WSW–ENE-trending branches, which form a conjugate set or two synthetic splays of anastomosing shear zones. The shear zones were the site of fluid flow and quartz vein emplacement associated with precious metal deposition. Quartz veins have been formed in several stages, and vein thickness varies from a few centimetres to about 1 m. The two major shear zones (main ore zones in Fig. 5) show a strong alteration around decimetre- to metre-thick auriferous quartz veins and are accompanied by additional parallel, narrower shear and alteration zones. The shear zones are characterized by a well-developed 45–60° NE- to NNE-dipping planar S-fabric. In addition to a mineral lineation (L_3 or L_4) and a NE-plunging crenulation

https://doi.org/10.1017/S0016756809990628 Published online by Cambridge University Press

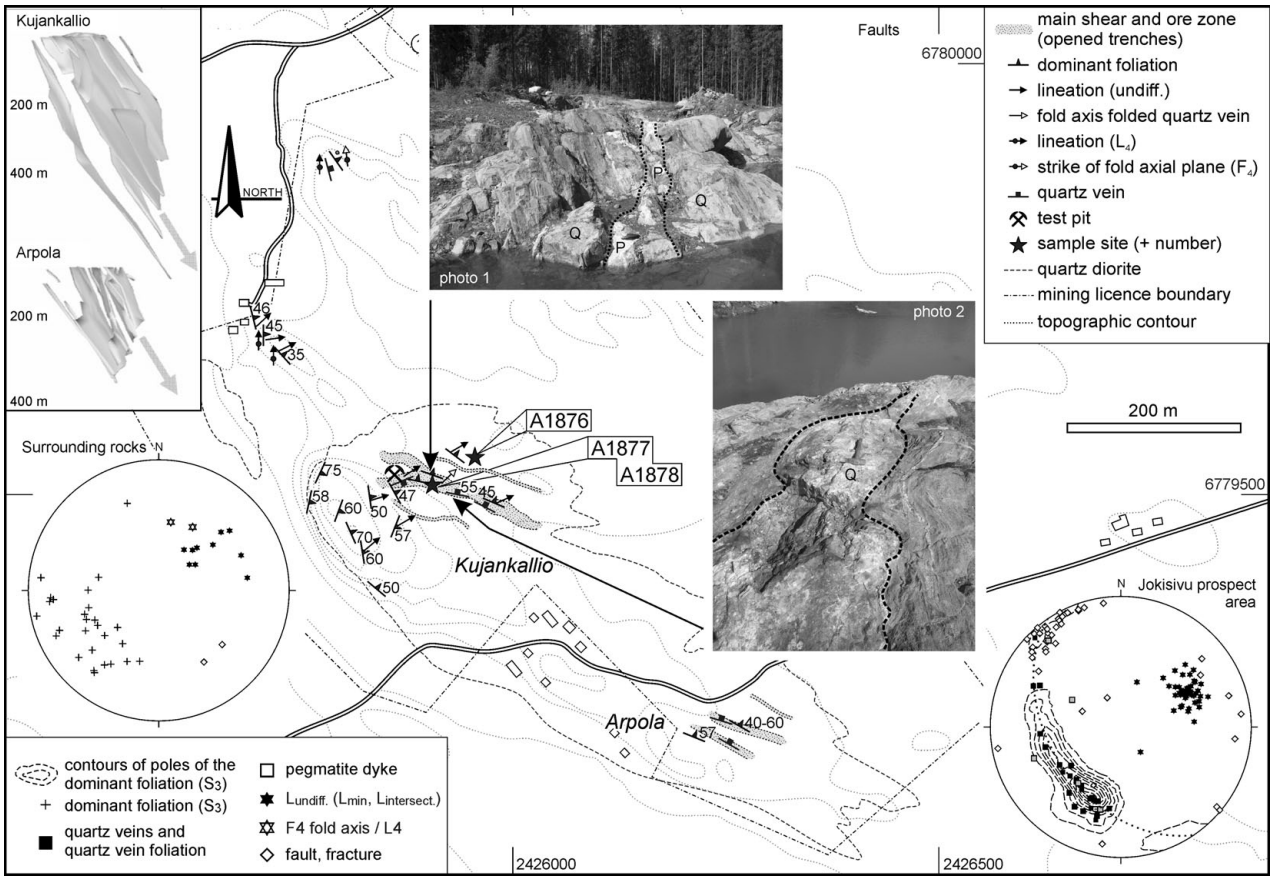

Figure 5. Map of the Jokisivu prospect area, including structural data and sample sites for dating (outline of the quartz diorite and the mining licence boundary is based on Dragon Mining NL, 2005). Photo 1: View towards the west to the sample site for the altered quartz diorite and the pegmatite dyke (A1877, A1878). The pegmatite (P) cuts the auriferous quartz veins (Q) and the dominant foliation (left = S); mine test pit in the back. Photo 2: Pinching and swelling gold mineralized quartz vein in the Kujankallio ore zone (length of hammer = ~ 64 cm, left = N). The inlet illustrates the Kujankallio and Arpola ore bodies comprising stacked NE- to NNE-dipping vein sets. Map coordinates: Finnish Grid (KKJ). Stereoplots: equal area lower hemisphere projection.

lineation (probably L_4), both also occurring in the unaltered host rock, the shear zone also displays a locally developed rodding lineation of stretched quartz, and an intersection lineation that is related to the intersection of the shear foliation and fractures with earlier foliation planes. These shear zone structures overprint the earlier D_3 and D_4 structures, indicating that the quartz vein emplacement and gold deposition post-date D_4. Luukkonen (1994), in contrast, suggests that the shear zones, and thus the ore zone, have been folded by F_2 (= F_4 in this paper). However, the overprinting relationships clearly point to a post-D_4 development. On the other hand, it is possible that D_6 shearing associated with gold mineralization partly reactivated a pre-existing D_3 shear zone.

Macroscopically well-developed shear sense indicators and a clear asymmetry of the fabrics are lacking, so that the kinematics of the D_6 shear zone cannot be inferred with certainty; however, the fabric suggests a strong co-axial flattening component. It cannot be excluded that the shear zone may be dilational rather than contractional.

D_6 shearing started at elevated temperatures with ductile deformation of the quartz dioritic host rock. Elongated, coarse-grained to pegmatititc quartzo-feldpatic dykes and patches intruded into the main shear zone and are locally boudinaged or folded. They represent early fluid batches of the hydrothermal fluid flow into the shear zone. The quartz veins were emplaced shortly after the quartz-feldspar dykes. With increasing distance from the main shear and ore zone, thickness, density and number of shear zones and quartz veins decrease. Alteration zones become more 'diffuse' and comprise spaced thin quartz veins accompanied by narrow anastomosing shear bands, of which some surround and locally cut the thick quartz veins of the main ore zone. They probably formed in the waning stages of shear deformation with progressive concentration of shearing in narrow zones. These relationships suggest a prolonged shearing and mineralization event.

The D_6 shear zones may be linked with (W)SW–(E)NE-trending dextral shear zones in the Häme and Uusimaa belts formed during late Svecofennian dextral transpression (Ehlers, Lindroos & Selonen, 1993; Nironen, 1999; Väisänen & Hölttä, 1999; Levin *et al.* 2005; Saalmann, 2007; Väisänen & Skyttä, 2007; Pajunen *et al.* 2008; Torvela, Mänttäri & Hermansson, 2008). NW–SE-trending shear zones west of the Pirkanmaa belt (Kynsikangas and Kankaanpää shear

https://doi.org/10.1017/S0016756809990628 Published online by Cambridge University Press

zones; Figs 1, 3) were also active at this time. The shear zones in the Jokisivu prospect probably branch from second or third order structures parallel to the major NW–SE structures.

2.b.4. Late-D_6 pegmatite dykes and quartz veins

A number of pegmatitic dykes partly follow the general strike of the ore zone. To the northwest, they leave the ore zone and clearly cut the dominant foliation of the quartz diorite. The dyke thickness ranges from a few centimetres to several decimetres. Different generations of dykes can be distinguished. Some dykes and patches pre-date the auriferous quartz veins since they are cut by them; the temperature during their emplacement was high. Other dykes show a narrow margin of biotite at the contact to the wall rock; some contain garnet. Some dykes show a shape-preferred orientation of biotite and of the long axes of large feldspar crystals forming a flaser-like foliation. Many dykes run at least partly sub-parallel to the NE-dipping shear zone foliation and it is likely that they were emplaced during the waning stages of shearing or shortly after deformation ceased. A slightly younger pegmatite dyke can be followed tens of metres along strike in the Kujankallio ore zone (Fig. 5, photo 1); however, it cuts the shear zone foliation as well as the auriferous quartz veins and thus post-dates quartz vein intrusion and the main gold mineralization stage. Its intrusion likely followed shortly after the quartz vein emplacement. This is supported by chemical analyses (Luukkonen, 1994) showing gold in the dyke, although the concentration is very low, and by the obtained age data (see Section 4). The dyke shows no signs of metamorphism or strong deformation, and quartz and feldspar crystals grew at right angles to the dyke walls. These features suggest that the intrusion of the pegmatite dykes occurred in a time span with decreasing temperature and shear strain.

Finally, the moderately NNE-dipping shear zone foliation and gold-bearing quartz veins locally show slickensides with 35–50° ENE-plunging slickenlines, which, together with steps on the slickenside surface, indicate a top-to-the-WSW directed transport.

2.b.5. Post-D_6 deformation

Subsequent deformation is characterized by faulting and fracturing during further decrease in temperature. Narrow SW–NE-trending sub-vertical to mostly steeply SE-dipping, unmineralized quartz veins cut the gold-bearing quartz veins and the pegmatites. They are associated with brittle faults showing dextral strike-slip movements, with some of them also having a slight normal dip-slip component. Different fault sets and the reactivation of pre-existing faults indicate several faulting episodes formed in different stress fields (Fig. 4). Unequivocal cross-cutting relationships of fault sets have not been found; their development requires a more detailed analysis.

2.c. Mineralization

The prospect comprises two ore zones, Kujankallio and Arpola, about 300 m apart. Gold occurs in quartz veins emplaced in shear zones (D_6) cutting the quartz diorite. Shearing was accompanied by fluid flow, and pinching-and-swelling and boudinaged quartz veins (Fig. 5, photo 2) imply that their emplacement occurred during progressive shearing.

Drilling and resource estimation showed that the Kujankallio and Arpola ore zones comprise a number of 50–60° NE- to NNE-dipping separate vein systems, which are stacked in a sub-parallel array (Grönholm, 2006). The Ag content is low; the relative abundance of Au and Ag is on average 97 % Au, 3 % Ag (Luukkonen, Grönholm & Hannila, 1992).

Gold mineralization occurs in quartz veins a few centimetres to a metre thick and surrounding mineralized alteration zones of a few decimetres to several metres width (Fig. 5, photo 1). The Arpola and Kujankallio vein sets have been drilled to the 350 m and 200 m level, respectively, and the latter has been estimated to extend to at least 500 m (Dragon Mining Ltd, 2007). The current *in situ* resource estimate is 1,473,000 tonnes of ore at an average grade of 6.8 g gold per tonne (Haga, 2005). The alteration is strongest in the main shear and ore zones (Fig. 5) displaying greenish–brownish to rusty colours. Alteration is characterized mainly by silicification and biotitization; skarn reactions have also been reported (Luukkonen, 1994; Grönholm, 2006). Sulphide minerals are common in the shear zone. To a much lesser extent, sericitization and chloritization can be observed. Garnet is quite common in the altered quartz diorite and close to mafic dykes within the alteration zone as well as in pegmatite dykes.

Typical ore minerals are gold, pyrrhotite, arsenopyrite, loellingite (mostly as inclusions in arsenopyrite), pyrite (mostly secondary after pyrrhotite), scheelite, Bi-tellurides and minor chalcopyrite and antimony minerals, as well as rare galena and sphalerite (Luukkonen, Grönholm & Hannila, 1992; Luukkonen, 1994; Grönholm, 2006). Pyrrhotite is the most common ore mineral, which also has been remobilized during later stages; arsenopyrite is very common as well, and several generations of this mineral have been reported by Luukkonen (1994). Gold occurs mainly as free grains (Luukkonen, 1994; Grönholm, 2006), often intergrown with tellurides as well as maldonite and aurostibite, sometimes it occurs as inclusion in scheelite, and it is also related to arsenopyrite and pyrrhotite (Luukkonen, 1994). Luukkonen (1994) reconstructed a series of mineral assemblages at Jokisivu, starting with crystallization of oxide minerals (like magnetite, ilmenite, and scheelite) at $T > 400$ °C, followed by two subsequent stages of sulphide deposition beginning with arsenopyrite, loellingite and

https://doi.org/10.1017/S0016756809990628 Published online by Cambridge University Press

pyrrhotite at temperatures between 300 and 400 °C, including first gold, and finally the precious metal mineralization at 200–300 °C.

3. Samples and dating methods

In order to bracket the age of the gold mineralization, samples have been taken that (1) pre-date mineralization (unmineralized host rock, sample A1876), (2) are overprinted by the mineralizing hydrothermal event (altered quartz diorite truncated by gold-bearing quartz veins, sample A1877), and (3) post-date the auriferous quartz veins (cross-cutting pegmatite dyke, sample A1878).

3.a. Sample A1876 Kujankallio-1

A sample of the unaltered quartz dioritic host rock outside the ore zone has been taken in Kujankallio. The sample is not truncated by quartz veins and shows no macroscopically visible extensive alteration.

The sample yielded a large amount of zircon grains forming a heterogeneous population. In the density fraction 3.6–4.0 g cm^{-3} a heterogeneous group of zircon grains comprises large, stubby and turbid, and long, thin and transparent grains, as well as some rounded grains and crystals. The 4.0–4.2 density fraction consists mostly of euhedral, long, mostly transparent, pale zircon grains, but in addition contains grains with different morphologies.

3.b. Sample A1877 Kujankallio-2

Sample A1877 is from the granitic pegmatite dyke that partly follows the ore zone in Kujankallio and cuts the auriferous quartz veins, and therefore post-dates the main gold mineralization stage; it shows reliable cross-cutting relationships necessary for data interpretation.

The zircon grains are long, euhedral and translucent to turbid. In the heaviest fraction ($\rho > 4.3$ g cm^{-3}), some Au and a few various zircon types were found. In addition, turbid to translucent monazite grains have been separated for TIMS U–Pb analysis.

3.c. Sample A1878 Kujankallio-3

The strongly altered quartz diorite sample has been taken from the inner ore zone in Kujankallio surrounding the auriferous quartz vein. The sample yielded zircon with needle-like to almost equidimensional grain shapes. The most common grain types are colourless, transparent to translucent and turbid, brownish elongated prismatic grains. The sample also contains translucent titanite suitable for U–Pb dating.

3.d. Analytical methods

Zircons and titanite were dated with an ion microprobe using the SIMS (secondary ion mass spectrometry) technique. In addition, monazite was analysed with the TIMS (thermal ionization mass spectrometry) method.

Zircon for U–Pb work was selected by hand-picking after heavy liquid and magnetic separation. The selected zircons were mounted in epoxy, polished, and coated with gold. The ion microprobe (SIMS) analyses were made using a Cameca IMS 1270, a Nordic facility at the Swedish Museum of Natural History, Stockholm, Sweden. The spot-diameter for the 5–7 nA primary O_2^- ion beam was ~ 20 μm, and oxygen flooding in the sample chamber was used to increase the production of Pb^+ ions. Three counting blocks, each including four cycles of the Zr, Pb, Th and U species of interest, were measured from each spot. The mass resolution ($M/\Delta M$) was 5400 (10 %). The raw data were calibrated against a zircon standard (91500; Wiedenbeck *et al.* 1995) and corrected for modern common lead ($T = 0$; Stacey & Kramers, 1975). For the detailed analytical procedure, see Whitehouse, Kamber & Moorbath (1999) and Whitehouse & Kamber (2005).

For titanite SIMS analysis, two counting blocks, each including five cycles, were measured and no oxygen flooding into the sample chamber was used. Titanite analyses used a similar routine to that used for zircon (omitting ^{208}Pb and ThO from the peak sequence); the $CaTi_2O_4$ peaks were used as a matrix reference at mass 200 and as a reference mass for ^{204}Pb. Pb/U ratios were calibrated relative to a titanite from the Kahn mine, Namibia (from the collections at the Swedish Museum of Natural History), which has an age of 518 Ma (MJW, unpub. data; Kinny *et al.* 1994 report an ID-TIMS concordant U–Pb age of 518 ± 2 Ma). The raw data were corrected for modern common lead ($T = 0$; Stacey & Kramers, 1975).

For multigrain ID-TIMS (isotopic dilution-thermal ionization mass spectrometry) U–Pb age determinations, the decomposition of monazite and titanite and extraction of U and Pb mainly followed the procedure described by Krogh (1973, 1982). ^{235}U–^{206}Pb (monazite) or ^{235}U–^{208}Pb (titanite) spiked and unspiked isotopic ratios were measured using a VG Sector 54 thermal ionization multicollector mass spectrometer. Based on repeated SRM981 standard runs, the measured lead isotopic ratios were normalized using fractionation correction of $0.10 \pm 0.05\%$ per a.m.u. Pb/U ratios were calculated using the PbDat-program (Ludwig, 1991). Plotting of the U–Pb isotope data, fitting of the discordia lines and calculation of the intercept and/or concordia ages were done using the program Isoplot/Ex (Ludwig, 2003). Age errors are calculated at 2σ with ignored decay constant errors. Data-point error ellipses in figures are 2σ. All TIMS U–Pb analyses were done at GTK, Espoo.

Analytical results are shown in Tables 1 and 2.

4. Analytical results

4.a. Sample A1876 Kujankallio-1

From sample A1876 Kujankallio-1 (unaltered quartz dioritic rock), a total of ten zircon domains were dated. The analyses were mostly done on typical euhedral,

https://doi.org/10.1017/S0016756809990628 Published online by Cambridge University Press

Table 1. Zircon and titanite SIMS U–Pb isotopic data for Kujankallio rock samples related to gold mineralization

Sample/ spot no.	Dated zircon domain	$^{207}Pb/^{206}Pb$	±σ	$^{207}Pb/^{235}U$	±σ	$^{206}Pb/^{238}U$	±σ	$^{207}Pb/^{235}U$	±σ %	$^{206}Pb/^{238}U$	±σ %	ρ (1)	Disc. % (2)	[U] ppm	[Th] ppm	[Pb] ppm	Th/U meas.	$^{206}Pb/^{204}Pb$ measured	f_{206} % (3)
Zircon U-Pb data																			
A1876 Kujankallio-1 quartz diorite (hosting the Au mineralization)/n2663																			
n2663-01a	Zoned (euhedral, short, with thin pale rim)	1905	6	1869	9	1836	17	5.298	1.1	0.3295	1.1	0.96	−1.7	393	204	165	0.52	8.55E+03	0.22
n2663-02a	Zoned (euhedral, long)	1883	6	1871	11	1860	20	5.313	1.3	0.3345	1.2	0.96		249	111	104	0.45	1.66E+05	{0.01}
n2663-03a	Zoned (euhedral, long)	1878	6	1849	9	1824	17	5.179	1.1	0.3270	1.1	0.95	−0.8	283	104	113	0.37	2.52E+05	{0.01}
n2663-04a	Zoned (euhedral, long)	1806	6	1788	10	1773	17	4.817	1.1	0.3165	1.1	0.96		456	48	165	0.10	5.71E+04	0.03
n2663-05a	Zoned (euhedral, long)	1883	4	1872	8	1861	14	5.318	0.9	0.3348	0.9	0.96		517	289	223	0.56	6.58E+04	0.03
n2663-06a	Zoned (euhedral, long)	1885	5	1867	8	1852	14	5.290	0.9	0.3328	0.9	0.96		482	260	205	0.54	1.94E+05	0.01
n2663-07a	Zoned (euhedral, long)	1885	7	1848	9	1817	15	5.175	1.0	0.3255	1.0	0.93	−1.6	208	78	83	0.37	4.29E+04	0.04
n2663-08a	Zoned (euhedral, long)	1883	4	1878	9	1873	17	5.355	1.1	0.3371	1.0	0.98		624	380	272	0.61	1.88E+05	0.01
n2663-10a	Zoned (euhedral, long)	1887	5	1872	8	1859	15	5.321	1.0	0.3343	0.9	0.96		500	264	213	0.53	3.39E+04	0.06
A1877 Kujankallio-2 pegmatite (post mineralization)/n2664																			
n2664-01a	Mostly homogeneous, medium dark	1710	5	1749	8	1782	14	4.599	0.9	0.3184	0.9	0.95	2.5	8455	233	2996	0.03	2.70E+03	0.69
n2664-02a	Mostly homogeneous, medium dark domain	1610	3	1539	7	1487	12	3.550	0.9	0.2595	0.9	0.99	−6.7	7986	268	2295	0.03	2.08E+03	0.90
n2664-02b	Mostly homogeneous, pale domain	1805	3	1816	9	1826	16	4.981	1.0	0.3274	1.0	0.99		1687	30	616	0.02	6.32E+05	0.00
n2664-03a	Mostly homogeneous, medium dark domain	1775	4	1787	8	1797	14	4.812	0.9	0.3216	0.9	0.97		3507	106	1258	0.03	2.98E+03	0.63
n2664-03b	Mostly homogeneous, pale domain	1804	3	1794	8	1786	14	4.853	0.9	0.3193	0.9	0.98		1657	43	591	0.03	3.01E+05	0.01
n2664-05a	Mostly homogeneous, medium dark	1870	2	1906	9	1939	16	5.536	1.0	0.3510	1.0	1.00	2.2	6543	209	2579	0.03	5.98E+03	0.31
n2664-06a	Mostly homogeneous, pale	1792	3	1801	8	1810	15	4.896	1.0	0.3241	1.0	0.98		1635	41	592	0.03	3.34E+04	0.06
n2664-08a	Mostly homogeneous, pale	1808	3	1830	8	1850	16	5.064	1.0	0.3324	1.0	0.99	0.6	2573	54	955	0.02	7.54E+04	0.02
n2664-08b	Mostly homog., medium dark, some alteration	1575	4	1522	7	1485	12	3.478	0.9	0.2590	0.9	0.97	−4.4	9396	268	2690	0.03	8.06E+03	0.23
n2664-09a	Homogeneous, pale	1810	3	1830	9	1848	16	5.062	1.0	0.3319	1.0	0.98	0.1	3560	62	1318	0.02	7.54E+04	0.00
n2664-10a	Homogeneous, pale inner domain	1803	5	1800	8	1798	14	4.888	0.9	0.3216	0.9	0.95		1344	31	483	0.02	1.71E+05	0.01
n2664-11a	Altered, zoning visible	1448	6	1109	7	945	9	1.982	1.1	0.1578	1.1	0.96	−35.3	5338	138	926	0.03	3.96E+03	0.47
n2664-12a	Homogeneous, medium dark inner domain	1807	2	1774	8	1745	14	4.735	0.9	0.3108	0.9	0.99	−2.2	5558	160	1932	0.03	1.01E+04	0.18
n2664-13a	Homogeneous, medium dark	1863	3	1864	8	1866	15	5.272	0.9	0.3357	0.9	0.99		5099	75	1915	0.01	1.32E+04	0.14
n2664-14a	Homogeneous, medium dark domain	1874	7	1929	9	1981	17	5.685	1.1	0.3598	1.0	0.93	3.9	1992	31	803	0.02	3.00E+04	0.06
n2664-14b	Homogeneous, pale domain	1812	4	1804	8	1797	14	4.910	0.9	0.3215	0.9	0.98		1493	23	535	0.02	6.02E+05	{0.00}
n2664-15a	Altered, zoning visible	973	5	616	4	523	4	0.834	0.9	0.0846	0.9	0.96	−45.9	9377	279	857	0.03	1.71E+04	0.11
n2664-16a	partially altered, pale domain	1782	6	1682	8	1602	12	4.239	0.9	0.2822	0.9	0.93	−9.2	2093	46	658	0.02	6.00E+03	0.31
A1878 Kujankallio-3 altered diorite/n2658																			
n2658-11a	Zoned	1885	7	1879	9	1874	15	5.363	1.0	0.3373	0.9	0.93		228	64	92	0.28	6.80E+04	0.03
n2658-12a	Homogeneous inner domain	1886	5	1881	9	1876	17	5.376	1.1	0.3378	1.0	0.97		432	172	180	0.40	2.01E+05	0.01
n2658-12b	Zoned rim	1887	8	1873	9	1861	15	5.328	1.0	0.3347	0.9	0.91		182	48	73	0.26	7.84E+04	0.02
n2658-13a	Zoned core	1876	6	1866	8	1857	14	5.284	0.9	0.3339	0.9	0.94		323	112	131	0.35	7.27E+04	0.03

Table 1. Continued.

Sample/ spot no.	Dated zircon domain	$^{207}Pb/^{206}Pb$	±σ	$^{207}Pb/^{235}U$	±σ	$^{206}Pb/^{238}U$	±σ	$^{207}Pb/^{235}U$	±σ %	$^{206}Pb/^{238}U$	±σ %	ρ (1)	Disc. % (2)	[U] ppm	[Th] ppm	[Pb] ppm	Th/U meas.	$^{206}Pb/^{204}Pb$ measured	f_{206} % (3)
n2658-13b	Homogeneous rim	1888	10	1888	11	1888	18	5.420	1.3	0.3402	1.1	0.90		130	26	52	0.20	1.32E+05	{0.01}
n2658-14a	Homogeneous core	1883	6	1891	10	1898	18	5.436	1.1	0.3423	1.1	0.95		314	110	131	0.35	6.34E+04	0.03
n2658-14b	Zoned rim	1876	12	1888	9	1898	14	5.418	1.1	0.3424	0.9	0.79		111	19	44	0.17	5.32E+04	0.04
n2658-15a	Darker core	1906	12	1880	10	1856	15	5.368	1.1	0.3336	0.9	0.81		88	18	35	0.20	2.11E+05	{0.01}
n2658-15b	Homogeneous rim	1888	6	1916	8	1942	15	5.601	1.0	0.3516	0.9	0.93	0.8	350	98	147	0.28	2.86E+04	0.07
n2658-16a	Zoned	1871	12	1839	9	1811	14	5.118	1.1	0.3243	0.9	0.79	−0.1	100	23	38	0.23	5.32E+03	0.35
n2658-17a	Homogeneous pale core	1881	6	1877	8	1873	14	5.351	0.9	0.3372	0.9	0.93		334	121	137	0.36	9.16E+04	0.02
n2658-17b	Zoned darker domain	1883	10	1880	9	1878	15	5.372	1.1	0.3383	0.9	0.86		128	24	50	0.19	1.79E+04	0.10
n2658-18a	Zoned	1887	6	1888	8	1890	15	5.422	1.0	0.3406	0.9	0.93		313	118	130	0.38	1.16E+05	0.02
n2658-19a	Mostly homogeneous core	1878	13	1865	10	1853	14	5.275	1.1	0.3331	0.9	0.77		266	100	108	0.38	2.22E+04	0.08
n2658-19b	Pale homogeneous rim	1794	4	1794	8	1794	14	4.854	0.9	0.3209	0.9	0.97		1418	44	509	0.03	1.42E+05	0.01
n2658-20a	Pale rim domain	1878	9	1871	9	1864	14	5.314	1.0	0.3354	0.9	0.87		257	85	103	0.33	2.88E+04	0.07
n2658-21a	Darker Mostly homog	1896	11	1867	9	1841	14	5.287	1.1	0.3305	0.9	0.82	−0.1	157	51	63	0.33	6.13E+04	{0.03}
n2658-21b	Pale domain	1883	10	1867	9	1853	14	5.289	1.1	0.3330	0.9	0.84		183	59	73	0.32	1.45E+05	{0.01}
n2658-22a	Pale homogeneous core	1893	9	1862	9	1834	14	5.259	1.0	0.3292	0.9	0.88	−0.8	303	105	121	0.35	1.85E+05	{0.01}
n2658-23a	Homogeneous	1877	9	1874	9	1872	14	5.334	1.0	0.3369	0.9	0.87		355	62	139	0.17	8.90E+04	0.02
n2658-24a	Homogeneous rim	1873	10	1863	9	1855	14	5.266	1.0	0.3335	0.9	0.85		311	119	126	0.38	1.20E+05	{0.02}
n2658-25a	Darker fractured outer domain	1877	24	1855	14	1836	14	5.215	1.6	0.3295	0.9	0.55		78	17	30	0.22	8.72E+03	0.21
n2658-25b	Pale homogeneous core domain	1876	8	1866	8	1857	14	5.282	1.0	0.3338	0.9	0.89		385	144	156	0.37	1.59E+04	0.12
n2658-26a	Pale homogeneous core	1877	6	1862	8	1849	14	5.259	0.9	0.3322	0.9	0.92		482	164	193	0.34	1.30E+05	0.01
n2658-27a	Darker core	1890	12	1873	10	1857	14	5.323	1.1	0.3338	0.9	0.79		135	41	54	0.31	4.22E+04	0.04
n2658-27b	Pale homogeneous rim	1811	4	1809	8	1808	14	4.941	0.9	0.3237	0.9	0.97		1384	34	501	0.02	7.24E+04	0.03
n2658-28a	Inner domain	1879	7	1889	13	1899	25	5.427	1.6	0.3425	1.5	0.97		311	95	127	0.31	2.91E+05	{0.01}
n2658-28b	Pale homogeneous rim	1887	4	1903	13	1918	26	5.514	1.6	0.3464	1.5	0.99		1064	228	433	0.21	5.04E+05	{0.00}
n2658-29a	Pale homogeneous	1887	5	1883	12	1879	23	5.387	1.4	0.3384	1.4	0.98		567	180	230	0.32	1.80E+05	{0.01}
n2658-30a	Darker inner	1879	9	1867	13	1856	22	5.287	1.5	0.3336	1.4	0.94		181	32	70	0.18	1.04E+04	0.18
n2658-30b	Pale rim domain	1826	3	1675	12	1558	21	4.205	1.5	0.2733	1.5	0.99	−13.9	1425	503	470	0.35	2.40E+04	0.08
Titanite U-Pb data																			
A1878 Kujankallio-3 altered diorite/n2658																			
n2658-01a	Darker domain	1796	18	1685	15	1598	21	4.258	1.8	0.2813	1.5	0.84	−7.2	75	23	26	75.4	1.91E+03	0.98
n2658-02a	Mostly homogeneous	1834	19	1700	15	1594	21	4.335	1.9	0.2805	1.5	0.81	−9.2	76	104	34	76.4	1.25E+03	1.50
n2658-03a	Paler inner domain (+dark rim)	1797	29	1702	18	1627	22	4.348	2.2	0.2870	1.5	0.68	−2.7	54	102	27	53.9	7.50E+02	2.49
n2658-04a	Darker homogeneous	1777	33	1691	20	1623	22	4.289	2.4	0.2863	1.5	0.64	−0.8	52	185	33	51.9	5.73E+02	3.27
n2658-05a	Darker homogeneous	1783	23	1682	17	1602	22	4.240	2.0	0.2821	1.5	0.77	−4.9	64	23	22	64.2	1.35E+03	1.39
n2658-06a	Paler homogeneous rim	1814	40	1722	23	1649	23	4.454	2.7	0.2914	1.6	0.57		43	135	27	43.3	5.63E+02	3.32
n2658-07a	Darker homogeneous	1791	26	1682	17	1597	22	4.244	2.1	0.2811	1.5	0.73	−5.1	70	18	24	70.4	1.30E+03	1.44
n2658-08a	Darker homogeneous	1684	47	1635	25	1598	21	4.005	3.0	0.2812	1.5	0.51		42	30	16	42.1	6.13E+02	3.05
n2658-09a	Paler inner domain (+dark rim)	1716	22	1577	16	1474	20	3.724	1.9	0.2570	1.5	0.77	−9.4	95	47	31	95.4	1.51E+03	1.24
n2658-10a	Paler (with scheelite inclusion)	1738	24	1621	16	1533	21	3.936	2.0	0.2684	1.5	0.76	−6.6	92	55	32	91.8	1.26E+03	1.48

All errors are at 1σ level.
(1) Error correlation in conventional concordia space.
(2) Age discordance at closest approach of error ellipse to concordia (2σ level).
(3) Percentage of common ^{206}Pb in measured ^{206}Pb, calculated from the ^{204}Pb signal assuming a present-day Stacey & Kramers (1975) model terrestrial Pb-isotope composition. Figures in brackets are given when no correction has been applied.

Table 2. Multigrain TIMS monazite U–Pb isotopic data

Sample information	Sample	U	Pb	$^{206}Pb/^{204}Pb$	$^{208}Pb/^{206}Pb$	Isotopic ratios[1]						Apparent ages (Ma ± 2σ)		
Analysed mineral and fraction	(mg)	(ppm)	(ppm)	measured	radiogenic	$^{206}Pb/^{238}U$	±2σ%	$^{207}Pb/^{235}U$	±2σ%	$^{207}Pb/^{206}Pb$	±2σ%	Rho[2]	$^{206}Pb/^{238}U$	$^{207}Pb/^{235}U$	$^{207}Pb/^{206}Pb$
A1877 Kujankallio-2 pegmatite															
Monazite, abraded 20 minutes	0.54	4528	8391	64000	5.50	0.3235	1.07	4.884	1.07	0.1095	0.072	0.99	1807	1800	1791 ± 2

[1] Isotopic ratios corrected for fractionation, blank (30 pg), and age related common lead (Stacey & Kramers, 1975; $^{206}Pb/^{204}Pb \pm 0.2$, $^{207}Pb/^{204}Pb \pm 0.1$, $^{208}Pb/^{204}Pb \pm 0.2$).
[2] Rho: Error correlation between $^{206}Pb/^{238}U$ and $^{207}Pb/^{235}U$ ratios. All errors are 2σ.

long prismatic zircons showing weak longitudinal zoning in BSE images. Eight analyses are nearly concordant or slightly discordant analyses and plot in a cluster. Seven of these (Fig. 6) determine a Pb–Pb mean age of 1884 ± 4 Ma for the Kujankallio sample. Only a single zircon grain could be analysed, which yields a ^{207}Pb–^{206}Pb age of 1806 ± 12 Ma.

4.b. Sample A1877 Kujankallio-2

From the pegmatite dyke a total of 20 zircon domains were dated from typical long prismatic and coarse-grained pegmatitic zircons. In BSE images the zircon grains show that they are metamict with varying degrees of dark alteration with minor paler domains. Despite the alteration, the initial magmatic zoning is still visible in some grains. The spot U–Pb analyses were mostly done on pale, less altered zircon domains, but dark altered domains were also dated for reference. All the analyses show low Th/U (~ 0.02–0.03).

On the concordia diagram (Fig. 6), three separate age groups can be distinguished. Zircons *c.* 1.86 Ga old are interpreted to be inherited. Nine concordant or slightly discordant analyses plot in a cluster with an age of approximately 1.8 Ga (Fig. 6). Four U–Pb analyses from altered or less altered domains plot on the *c.* 1.6 Ga reference line, which indicates that the rocks in this area have been affected by younger rapakivi intrusion and related processes of that age.

Translucent monazite grains have been chosen for conventional TIMS U–Pb analysis to get further age constraints (Table 2). The result of 1792 ± 3 Ma is comparable with the zircon data and gives the minimum or approximate crystallization age of the pegmatite.

4.c. Sample A1878 Kujankallio-3

A total of 31 zircon domains (rim and core domains) were dated from the altered quartz diorite sample taken from the gold-bearing shear zone. Most of the analyses are either concordant or only slightly discordant and the common lead proportions are low. Analyses from zoned, elongated zircons and those from core domains, as well as most of the rim analyses, plot in a cluster in the concordia diagram (Fig. 6). The concordia age of 1881 ± 3 Ma is determined by 24 of 28 analyses, and this age coincides with the 1884 ± 4 Ma age determined for unaltered host-rock sample A1876 Kujankallio-1.

From paler and structurally homogeneous rim domains (BSE images, Fig. 6), a concordia age of 1802 ± 15 Ma can be calculated for two low Th/U concordant analyses.

Ten SIMS U–Pb analyses were performed on titanites from the alteration zone. Most of the data are discordant, and therefore a reasonable U–Pb age could not be calculated. However, a ^{207}Pb–^{206}Pb mean minimum age estimate of 1801 ± 18 Ma for the mineralization-related alteration could be calculated for the titanite using seven ^{207}Pb–^{206}Pb ages (Fig. 6).

https://doi.org/10.1017/S0016756809990628 Published online by Cambridge University Press

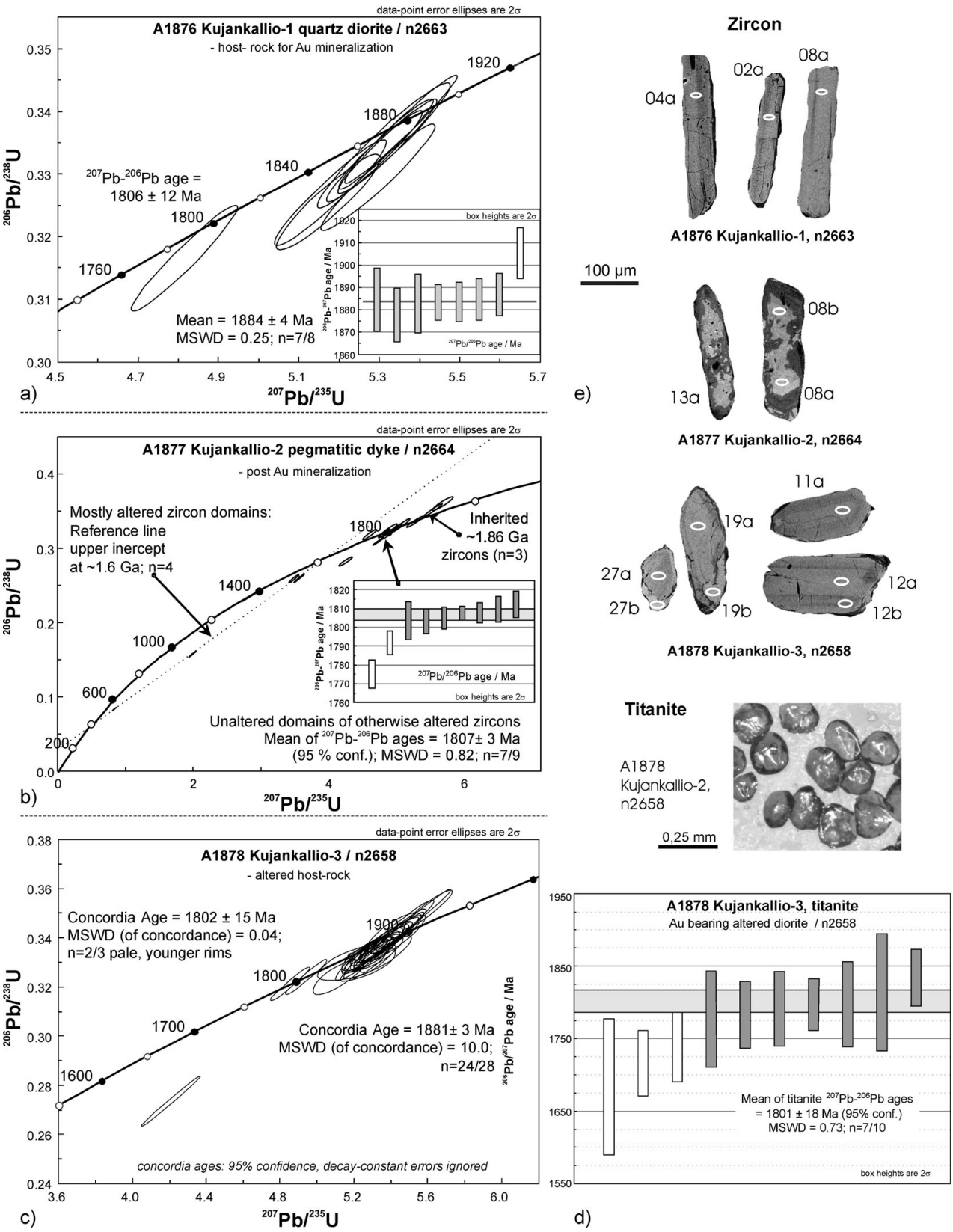

Figure 6. (a) Concordia plot of zircon SIMS U–Pb isotopic data, A1876 Kujankallio-1 unaltered volcanic rock hosting the Au mineralization. Inset shows the distribution and the mean of ^{207}Pb–^{206}Pb ages. (b) Concordia plot of zircon SIMS U–Pb isotopic data, A1877 Kujankallio-2 pegmatitic dyke. Inset shows the distribution and the mean of ^{207}Pb–^{206}Pb ages from the pegmatitic zircons. (c) Concordia plot of zircon SIMS U–Pb isotopic data, A1878 Kujankallio-3 altered quartz diorite. (d) Diagram showing titanite ^{207}Pb–^{206}Pb ages and the corresponding mean age, altered host-rock sample A1878. (a–c) zircon ages, (d) titanite age; (e) BSE images of selected zircons and photo of titanite grains.

https://doi.org/10.1017/S0016756809990628 Published online by Cambridge University Press

Despite the large error, this age corresponds well with (1) the ages obtained from zircon rims from the same sample, (2) the age of the pegmatitic dyke (A1877 Kujankallio-2) post-dating the main mineralization stage, but having been emplaced in the late stages of the event, and (3) the younger age group observed in the unaltered quartz diorite host rock (A1876).

5. Discussion

5.a. U–Pb data summary and interpretation

The 1884 ± 4 Ma and 1881 ± 3 Ma zircon ages of the unaltered and altered quartz diorite, respectively, give a well-defined crystallization and intrusion age of the host rock. It defines the maximum age of gold mineralization in the Jokisivu prospect.

The 1802 ± 15 Ma age that has been detected from low Th/U rim domains of zircons from the altered quartz diorite age is similar to the 1807 ± 3 Ma age of the pegmatite, interpreted to determine the age of its emplacement, as well as the *c.* 1.80 Ga mean of ^{207}Pb–^{206}Pb titanite ages obtained from the altered quartz diorite wall rock. The closure temperature for diffusion in titanite is poorly known; estimates range from about 500 °C for resetting during metamorphism (Gascoyne, 1986) to > 650 °C (Scott & St-Onge, 1995; Schärer, Zhang & Tapponnier, 1994; Essex *et al.* 1997) or 700 °C (Verts, Chamberlain & Frost, 1996) and even > 700 °C (Pidgeon, Bosch & Bruguier, 1996). Frost, Chamberlain & Schumacher (2000) consider that titanite is reactive during metamorphism, suggesting that titanite U–Pb ages are likely to be reset at low temperatures by growth of new grains, rather than by diffusion. These authors calculate a closure temperature of 660 to > 700 °C, depending on grain size and cooling rate (10 °C/Ma and 100 °C/Ma, respectively). In conclusion, titanite U–Pb ages will record crystallization of grains at medium to high temperature and therefore could serve as a geochronometer for hydrothermal and metamorphic processes (Frost, Chamberlain & Schumacher, 2000).

Titanite occurs exclusively in the alteration zone and not in the unaltered host-rock, so it probably dates a metamorphic or a hydrothermal event. The obtained *c.* 1.80 Ga age could indicate a young metamorphic event or just continued metamorphism after the metamorphic peak. Temperatures started to decrease after D_4; however, it is possible that temperatures remained above 650 °C before the onset of shear zone formation in the Jokisivu prospect, so that the U–Pb system stayed open for a considerable time span until at *c.* 1.82–1.78 Ga temperatures dropped below 650–600 °C. This would also explain the absence of older metamorphic ages if the temperature did not change considerably for a long time span.

On the other hand, the titanite age may also represent a hydrothermal event that caused growth of new titanite and/or resetting of the titanite U–Pb system of earlier grains, as well as the growth of rims around zircon core domains in the altered quartz diorite. The age is similar to the crystallization age of the pegmatite dyke, supporting the structural interpretation that the pegmatite intrusion occurred during the late stages of mineralization, so that the obtained ages reflect both the magmatic pegmatite event as well as contemporaneous hydrothermal fluid flow through the shear zone. Shearing and mineralization started at high temperatures (see Section 2.b.4). In this scenario, the 1.82–1.79 Ga age obtained from zircon rims and titanite of the altered zone therefore dates the mineralization event. Since gold precipitation took place at temperatures between 200 and 400 °C (Luukkonen, 1994), the titanite age in Kujankallio serves as an upper age limit for the gold deposition; however, taking into account the age of the cross-cutting pegmatite dyke being emplaced during the late stages of the mineralization, 1.80 Ga should give the minimum age for the Au mineralization.

5.b. The relationship of gold mineralization to the structural evolution

Figure 4 attempts to correlate the structural evolution with (1) the Loimaa area (Nironen, 1999) south of the study area (Häme belt) and (2) the Pirkanmaa belt (Kilpeläinen, 1998). This correlation is used in the following discussion for further age constraints on the deformation.

Quartz dioritic to gabbroic rocks of 1.88 Ga also occur in the Prikanmaa belt (Kilpeläinen, 1998; Rutland, Williams & Korsman, 2004). The Hyyvinkää gabbro massifs in the Uusimaa belt likewise show an approximately similar 1.88–1.87 Ga age (Patchett & Kouvo, 1986). Since the quartz diorite at Jokisivu is affected by D_3, its 1.88 Ga age also gives a maximum age for the onset of this deformation. D_3 was accompanied by HT metamorphism resulting in migmatization. Leucosome veins like those in the mica gneisses in Jokisivu have also been observed in the Loimaa area, where the *c.* 1.87 Ga old Pöytyä granodiorite (PG in Fig. 1) is considered to have been emplaced during D_3 (Nironen, 1999). If this interpretation is correct, the age of D_3 and related HT metamorphism in this area is *c.* 1.87 Ga old and belongs to the early Svecofennian stage. In the Pirkanmaa belt, the age of migmatization has been obtained from *c.* 1878 Ma (Mouri, Korsman & Huhma, 1999) and 1880 ± 6 Ma (Rutland, Williams & Korsman, 2004) monazite ages, which overlap with the age of the Pöytyä graniodiorite. Inherited *c.* 1.86 Ga zircon grains found in sample Kujankallio-2 A1877 may have formed during this D_3 event.

The Oripää granite (OG in Fig. 1) is interpreted by Nironen (1999) to have been emplaced in the late stages of D_4. Unfortunately, the granite contains heterogeneous zircon populations, and their age data show large errors (Nironen, 1999; Kurhila *et al.* 2005) so that the age of the granite can only be roughly estimated between 1.86 and 1.80 Ga.

https://doi.org/10.1017/S0016756809990628 Published online by Cambridge University Press

Post-peak metamorphic shearing (D_6), quartz vein emplacement and related mineralization in Jokisivu occurred at 1.82–1.78 Ga. The obtained age data and the structural relationships show that gold mineralization can be linked to the late Svecofennian tectonic cycle and support the correlation with approximately WNW–ESE dextral transpression in the Häme and Uusimaa belts. In the Uusimaa belt, late Svecofennian development is characterized by granulite facies metamorphism and voluminous granite formation, whereas most areas in the Häme belt were affected by amphibolite facies metamorphism. Peak metamorphic conditions (750–800 °C, 4–5 kbar) were reached at 1830–1815 Ma in the western Uusimaa belt (U–Pb monazite; Mouri *et al.* 2005). Oblique contraction started from *c.* 1825 Ma onward (Skyttä, 2007).

Depending on the precise orientation to the shortening axes, NW–SE- and WNW–ESE-trending structures may show dilational (oblique extensional) kinematics with a sinistral component along the former set. Particularly when crossing the ductile–brittle boundary these structures would serve as main fluid conduits. Oblique extensional shear may also explain the scarcity of clear shear-sense indicators at Jokisivu, which would be expected, for example, in typical oblique contractional shear zones. The moderate dip to the NNE is not characteristic for strike-slip regimes but indicates an oblique dip-slip component.

Fluid flow was focused into the approximately NW–SE- to WNW–ESE-trending shear zones in Jokisivu, and in turn led to further localization and concentration of the shear deformation in these zones. NW–SE-trending shear zones and associated quartz veins also occur in the country rocks outside the Jokisivu prospect, for example, in intermediate porphyric metavolcanic rocks about 1.2 km SW of the Jokisivu deposit; however, a strong mineralization and alteration is absent. At Ritakallio, located about 5 km ESE of Jokisivu (Fig. 3b), a quartz dioritic to gabbroic body similar to the Jokisivu host rock also hosts moderately NE- to NNE-dipping gold-rich quartz veins in shear zones (Vuori *et al.* 2005). This implies that these plutonic bodies played an important role for the mineralization. A possible explanation is the rheological behaviour of these rocks. The titanite ages indicate that temperatures exceeded 550–650 °C at the beginning of shearing, which is high enough for ductile deformation of the host rock. Due to competence contrast to the surrounding mica gneisses, the quartz diorites and gabbros formed more rigid bodies with semi-ductile deformational behaviour already at higher temperatures. As a result of further cooling, the ductile–brittle boundary for the deformation behaviour of the quartz diorite was crossed while deformation continued. Hence, it showed localized shearing and fracturing during contraction in contrast to ongoing penetrative ductile deformation of the wall rocks, so that the permeable shear zones and fractures served as pathways as well as precipitation sites for mineralizing fluids.

The gold-bearing quartz veins precipitated from mineralizing fluids that intruded into the shear zone during active deformation. The cross-cutting steep SW–NE-trending and barren quartz-filled faults forming after the main stage of mineralization may be explained by increasing localization of the deformation into narrow (dextral) strike-slip shear and fault zones during progressive cooling. Similar features can be observed in the Häme and Uusimaa belts further south where the strain became increasingly localized into dextral strike-slip shear and fault zones after peak metamorphism (e.g. Nironen, 1999; Väisänen & Hölttä, 1999; Levin *et al.* 2005; Saalmann, 2007; Väisänen & Skyttä, 2007; Torvela, Mänttäri & Hermansson, 2008).

The described structural relationships suggest that shearing and fluid flow at Jokisivu took place over a prolonged time-span while temperatures were decreasing. This post-peak metamorphic setting is in accordance with mineralogical studies by Luukonen (1994) and Grönholm (2006). The structural control of mineralization and its spatial association with shear zones and auriferous quartz veins formed in a metamorphic terrain during the retrograde stages of orogenic evolution are typical of mesothermal orogenic gold deposits *sensu* Groves *et al.* (1998).

5.c. Regional implications

The Jokisivu prospect is located in the boundary zone between the Häme and Pirkanmaa belts. Although the structural evolution can be correlated with both areas, structures can be more easily compared with and traced to the Loimaa area further south, and together with the higher proportion of metavolcanic rocks, this may suggest that the Jokisivu area is part of the Häme belt rather than the Pirkanmaa belt.

During approximately WNW–ESE-oriented D_6 shortening, major NW–SE-trending shear zones (e.g. the Kynsikangas and Kankaanpää shear zones; Figs 1, 3) very likely played a major role in fluid flow. The shear zones in the Jokisivu prospect probably branch from second or third order structures parallel to the major NW–SE structures. The distribution of orogenic gold occurences in the Svecofennian domain of southern Finland shows striking alignments along NW–SE trend-lines, in particular in the Pirkanmaa belt but also in southern and central Ostrobothnia (Fig. 2). The majority of orogenic-type gold occurrences are indeed located close to NW–SE-trending shear zones (Eilu, 2007). NW–SE- and (W)SW–(E)NE-striking shear and fault zones are also important for some gold occurrences in the Häme belt (Saalmann, 2007). Moreover, the age of structurally controlled gold mineralization in this zone can be estimated at 1.83–1.80 Ga (Saalmann *et al.* 2008) and overlaps with the age in the Jokisivu prospect. The apparent absence of orogenic gold in the Uusimaa belt may partly result from difficulties identifying overprinting orogenic-type gold mineralization on metamorphosed epithermal deposits. On the other hand, granulite facies

https://doi.org/10.1017/S0016756809990628 Published online by Cambridge University Press

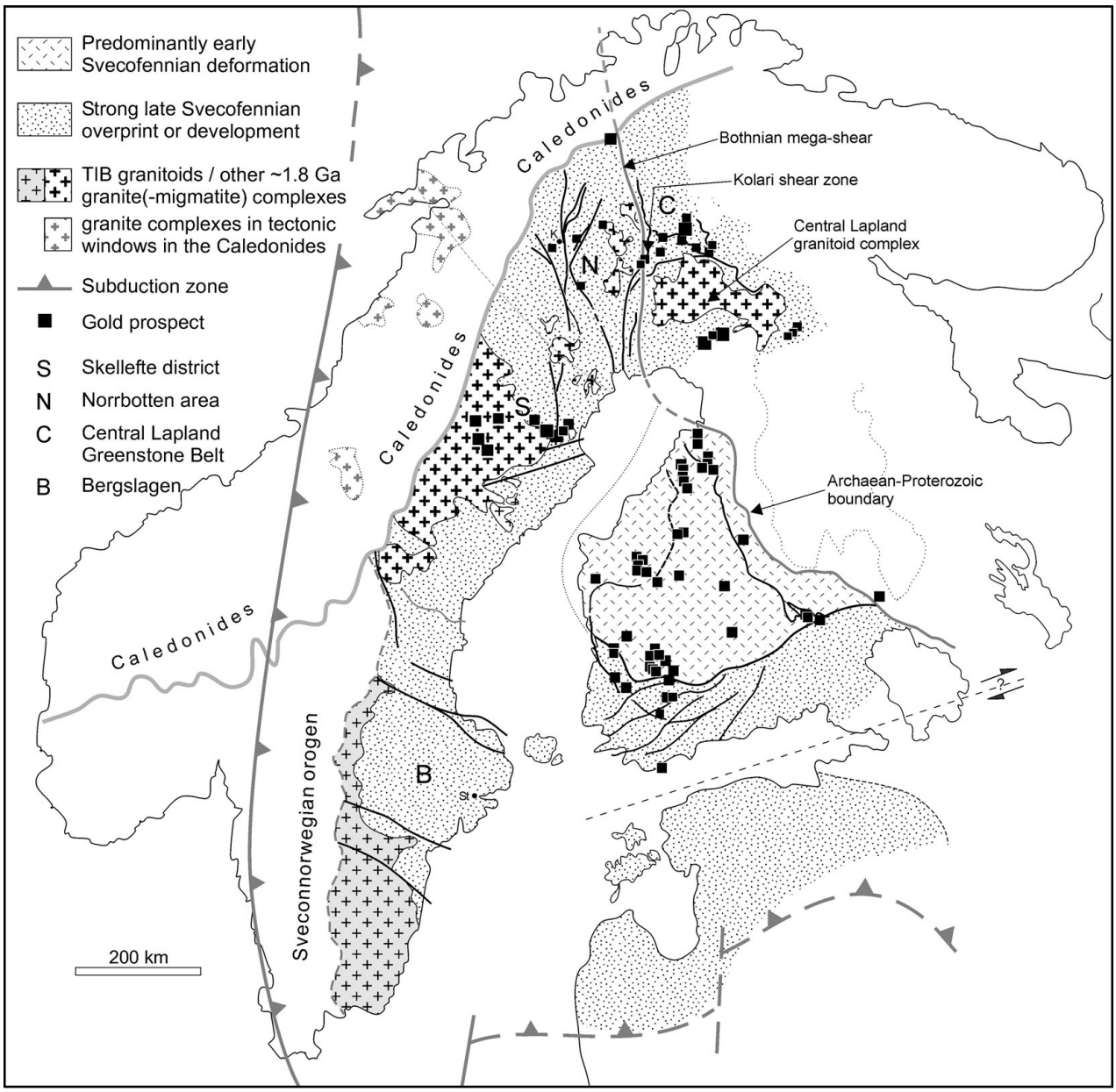

Figure 7. Tectonic scenario for the *c.* 1.82–1.78 Ga late Svecofennian tectono-magmatic and hydrothermal development related to a Cordilleran-type margin. Shear zones in Sweden after Bergman, Kübler & Martinsson, 2001; Weihed *et al.* 2002; Hermansson *et al.* 2007; in Finland after Korsman *et al.* 1997; distribution of TIB granitoids after Högdahl, Andersson & Eklund, 2004, and Weihed *et al.* 2002; gold occurrences after Eilu (2007) and Eilu *et al.* (2007). Note that the age of many gold occurrences is not well constrained and that not all prospects in this map necessarily belong to the 1.8 Ga late Svecofennian gold mineralization. K – Kiruna; St – Stockholm.

metamorphism and granitoid intrusions are partly coeval to mineralization in Jokisivu implying that the crust in the south may still have been too hot. In cooler areas further north, deformation was, in contrast, more strongly localized into shear zones with oblique-slip movements showing enhanced permeability compared to the surrounding rocks, which enabled concentrated fluid flow. Furthermore, these regions already crossed the ductile–brittle boundary, giving rise to brittle fracturing that provided conduits and pathways for fluid infiltration and percolation. This would explain the NW–SE trend line of gold occurrences, provided that they have formed during the same event. In this case the tectonic setting during the period 1.82–1.79 Ga would represent the most important event for orogenic gold mineralization in the Svecofennian domain of southern Finland.

Late Svecofennian shearing, metamorphism and contemporaneous *c.* 1.8 Ga old magmatism play an important role for mineralization in northern Finland and Sweden as well. Mineralization (iron oxide copper gold) in the Kolari shear zone in Finnish Lapland (Fig. 7) took place during thrusting at *c.* 1.8 Ga (Niiranen, Poutiainen & Mänttäri, 2007). Patison (2007) notes an important association between gold mineralization and shear zones post-dating the main regional peak metamorphism in the Central Lapland greenstone belt further east. The structural relationship

https://doi.org/10.1017/S0016756809990628 Published online by Cambridge University Press

to the Kolari shear zone is not well studied; however, if thrusting took place at the same time, at least part of the gold mineralization in central Lapland would have an age of *c.* 1.8 Ga as well. In the Norrbotten area in northern Sweden, NNE- to NNW-trending dextral shear zones that formed during E–W shortening (Bergman, Kübler & Martinsson, 2001) host copper–gold and gold mineralization, and they are comparable to the Kolari shear zone. This is confirmed by 1.80–1.78 Ga U–Pb titanite and monazite and ≤ 1.78 Ga hornblende Ar–Ar ages (Billström, Bergman & Martinsson, 2002).

A temporal relationship between *c.* 1.8 Ga voluminous granite magmatism (Revsund suite) and major N–S-trending ductile shear zones and gold mineralization also exists in the Skellefte district (Bergman-Weihed, 2001; Weihed *et al.* 2002; Bark, Broman & Weihed, 2007). The steep shear zones show reverse movements compatible with E–W shortening (Weihed *et al.* 2002) and are thus comparable to the shear zones in Norrbotten and the Kolari region. Dextral transpression at around 1.82 Ga (Högdahl & Sjöström, 2001), pegmatite intrusions with ages of 1.80–1.77 Ga (Romer & Smeds, 1997) and auriferous quartz veins in shear zones suggest a tectonic environment for mineralization similar to that in southern Finland.

In summary, many orogenic gold deposits in the Fennoscandian Shield formed after peak metamorphism and are structurally controlled by shear zones that formed in transpressional regimes associated with voluminous *c.* 1.8 Ga granitoid magmatism. Their distribution spreading from southern Finland and Sweden to Lapland in the north suggest a shield-wide tectono-magmatic and hydrothermal event, which in turn implies a comparable plate tectonic setting and control on mineralization.

It is beyond the scope of this paper to discuss various models for the tectonic evolution of southern Finland. In any case, the 1.82–1.78 Ga gold mineralization in Finland and Sweden took place during oblique contraction with E–W- to WNW–ESE-oriented shortening associated with widespread and voluminous granitoid magmatism, so that deformation was accompanied by high heat flow. Magmatism and metamorphism, reaching granulite facies conditions in some regions, started in extensional regimes (Korja & Heikkinen, 1995; Skyttä, 2007; Pajunen *et al.* 2008). Subsequent shortening beginning close to peak metamorphism affected a hot and partially molten crust and led to crustal stacking and thickening followed by immediate cooling of the lithosphere. In southern Finland these events represent the final stages of the Svecofennian orogenic evolution followed by cooling and (oblique) extension during orogenic collapse and stabilization.

Tectonic scenarios have to take into account the high heat flow as well as the cyclic orogenic evolution comprising two contractional episodes with HT metamorphism. Early Svecofennian deformation was followed by a period of uplift, erosion and sediment deposition at *c.* 1.85–1.83 Ga, which in turn was followed by renewed (late Svecofennian) contraction and metamorphism that also affected the post-1.86 Ga sedimentary rocks. Such episodic changes in stress can occur in subduction zone settings. It is suggested here that a subduction zone system and Cordilleran-type continental margin formed after the early Svecofennian accretionary events when the plate system was reorganized and the subduction system retreated further to the southwest and west. The subduction zone would have extended west of Sweden to the Baltic States (Fig. 7) because active continental margin magmatism at 1.85–1.78 Ga is also recorded in Lithuania (Skridlaite & Motuza, 2001) and in parts of the Mazowsze massif in northern Poland (Wiszniewska, Krzeminska & Dörr, 2007). Asthenospheric upwelling in the back-arc region (Finland, many parts of Sweden) as a response to slab rollback could have provided the high heat input, serving as a driving mechanism for magmatic and metamorphic events. In such a setting, a rapid tectonic switch from extension to contraction is triggered by a change from slab retreat (or rollback) to flat subduction, with the latter being initiated by arrival of a positively buoyant fragment (e.g. an oceanic plateau or continental crust) at the subduction zone causing contraction in the upper plate (e.g. Collins, 2002).

Subduction of oceanic crust enabled influx of hot asthenosphere and would provide the heat supply for shield-wide *c.* 1.8 Ga magmatism, metamorphism and hydrothermal precious metal mineralization. In the area affecting southern Finland, subduction was locking up since there is no significant deformation after 1.78 Ga, whereas subduction continued further west, as recorded in the younger, < 1.77 Ga, suites of the Transscandinavian Igneous Belt in Sweden, possibly after renewed migration of the subduction zone outwards. Post-orogenic (1.81–1.77 Ga) calc-alkaline and shoshonitic magmatism in southern Finland (Eklund *et al.* 1998; Andersson *et al.* 2006) may have been enabled by final slab break-off.

Acknowledgements. The authors would like to thank Polar Mining Oy/Dragon Mining NL for the permission to study the Jokisivu gold deposit. M. Karhunen, S. Mäenluoma and L. Järvinen are thanked for rock crushing and mineral separation. We are grateful to T. Hokkanen and A. Pulkkinen for laboratory work and mass spectrometry (TIMS). We also thank the personnel of the NORDSIM laboratory, L. Ilyinsky and K. Lindén, for assistance during different stages of sample preparation, analysis and data reduction. The ion microprobe facility in Stockholm (Nordsims) is operated under an agreement between the joint Nordic research councils (NOS-N), the Geological Survey of Finland and the Swedish Museum of Natural History. This is NordSIM contribution number 240. K.S. would like to express thanks to H. Arkimaa for processing the aeromagnetic map and an introduction to ErMapper. We greatly appreciate the helpful reviews of Ulf Söderlund and an anonymous referee, as well as suggestions made by the editor D. Pyle, which improved the manuscript. We also express our thanks to J. Holland for further editorial handling. This is a contribution to the

project 'Geological and metallogenic bedrock modelling' of the Geological Survey of Finland.

References

ALLEN, R. L., LUNDSTRÖM, I., RIPA, M., SIMEONOV, A., CHRISTOFFERSON, H. 1996. Facies analysis of a 1.9 Ga, continental margin, back-arc, felsic caldera province with diverse Zn–Pb–Ag–(Cu–Au) sulfide and Fe oxide deposits, Bergslagen region, Sweden. *Economic Geology* **91**, 979–1008.

ANDERSSON, U. B., EKLUND, O., FRÖJJDÖ, S. & KONOPELKO, D. 2006. 1.8 Ga magmatism in the Fennoscandian Shield; lateral variations in subcontinental mantle enrichment. *Lithos* **86**, 110–36.

BARK, G., BROMAN, C. & WEIHED, P. 2007. Fluid chemistry of the Palaeoproterozoic Fäboliden hypozonal orogenic gold deposit, northern Sweden: evidence from fluid inclusions. *Geologiska Föreningens i Stockholm Förhandlingar (GFF)* **129**, 197–210.

BERGMAN-WEIHED, J. 2001. Palaeoproterozoic deformation zones in the Skellefte and Arvidsjaur areas, northern Sweden. In *Economic geology research, Volume 1, 1999–2000* (ed. P. Weihed), pp. 46–68. *Sveriges Geologiska Undersökning Research Paper* **C 833**.

BERGMAN, S., KÜBLER, L. & MARTINSSON, O. 2001. Description of regional geological and geophysical maps of northern Norrbotten county (east of the Caledonian orogen). *Sveriges Geologiska Undersökning* **Ba 56**, 110 pp. Uppsala.

BILLSTRÖM, K., BERGMAN, S. & MARTINSSON, O. 2002. Post-1.9 Ga metamorphic, mineralization and hydrothermal events in northern Sweden. (Extended Abstract). *Geologiska Föreningens i Stockholm Förhandlingar (GFF)* **124**, 228.

COLLINS, W. J. 2002. Hot orogens, tectonic switching, and creation of continental crust. *Geology* **30**, 535–8.

DRAGON MINING LTD. 2007. *Annual Report 2006*. Perth, 86 pp. Link to source is available from the Geological Survey of Finland database: http://en.gtk.fi/ExplorationFinland/Commodities/Gold/jokisivu.html

DRAGON MINING NL. 2005. *Annual Report 2004*. Perth, 80 pp. Link to source is available from the Geological Survey of Finland database: http://en.gtk.fi/ExplorationFinland/Commodities/Gold/jokisivu.html

EHLERS, C., LINDROOS, A. & SELONEN, O. 1993. The late Svecofennian granite–migmatite zone of southern Finland – a belt of transpressive deformation and granite emplacement. *Precambrian Research* **64**, 295–309.

EILU, P. 2007. FINGOLD: Brief description of all drilling-indicated gold occurrences in Finland – The 2007 data. *Geological Survey of Finland Report of Investigation* **166**, 37 pp. Internet-link: http://en.gtk.fi/ExplorationFinland/Commodities/Gold/gtk_gold_map.html

EILU, P., HALLBERG, A., BERGMAN, T., FEOKTISTOV, V., KORSAKOVA, M., KRASOTKIN, S., LAMPIO, E., LITVINENKO, V., NURMI, P. A., OFTEN, M., PHILIPPOV, N., SANDSTAD, J. S., STROMOV, V. & TONTTI, M. 2007. Fennoscandian Ore Deposit Database Explanatory remarks to the database. *Geological Survey of Finland Report of Investigation* **168**, 17 pp. Internet-link: http://en.gtk.fi/ExplorationFinland/fodd/.

EILU, P., SORJONEN-WARD, P., NURMI, P. & NIIRANEN, T. 2003. A review of gold mineralization styles in Finland. *Economic Geology* **98**, 1329–54.

EKLUND, O., KONOPELKO, D., RUTANEN, H., FRÖJDÖ, S. & SHEBANOV, A. D. 1998. 1.8 Ga Svecofennian post-collisional shoshonitic magmatism in the Fennoscandian shield. *Lithos* **45**, 87–108.

ESSEX, R. M., GROMET, L. P., ANDREASSON, P. G. & ALBRECHT, L. 1997. Early Ordovician U–Pb metamorphic ages of the eclogite-bearing Seve Nappes, Northern Scandinavian Caledonides. *Journal of Metamorphic Geology* **15**, 665–76.

FROST, B. R., CHAMBERLAIN, K. R. & SCHUMACHER, J. C. 2000. Sphene (titanite): phase relations and role as a geochronometer. *Chemical Geology* **172**, 131–48.

GASCOYNE, M. 1986. Evidence for the stability of potential nuclear waste host, sphene, over geological time, from uranium–lead ages and uranium series disequilibrium measurements. *Applied Geochemistry* **1**, 199–210.

GRÖNHOLM, P. 2006. The Jokisivu gold deposit, southwest Finland. *Geological Society of Finland Bulletin* **1** (Spec. Issue), 42.

GROVES, D. I., GOLDFARB, R. J., GEBRE-MARIAM, M., HAGEMANN, S. G. & ROBERT, F. 1998. Orogenic gold deposits: A proposed classification in the context of their crustal distribution and relationship to other gold deposit types. *Ore Geology Reviews* **13**, 7–27.

HAGA, I. 2005. Dragon Mining's activities and strategies in Fennoscandia. FEM2005 Congress, Rovaniemi, 1–2 Dec 2005. Link to source is available from the Geological Survey of Finland FINGOLD database http://en.gtk.fi/ExplorationFinland/Commodities/Gold/jokisivu.html

HAKKARAINEN, G. 1994. Geology and geochemistry of the Hämeenlinna-Somero volcanic belt, southwestern Finland: a Paleoproterozoic island arc. In *Geochemistry of Proterozoic supracrustal rocks in Finland* (eds M. Nironen & Y. Kähkönen), pp. 85–100. Geological Survey of Finland, Special Publication no. 19.

HERMANSSON, T., STEPHENS, M. B., CORFU, F., ANDERSSON, J. & PAGE, L. 2007. Penetrative ductile deformation and amphibolite-facies metamorphism prior to 1851 Ma in the western part of the Svecofennian orogen, Fennoscandian Shield. *Precambrian Research* **153**, 29–45.

HÖGDAHL, K., ANDERSSON, U. B. & EKLUND, O. (eds) 2004. *The Transscandinavian Igneous Belt (TIB) in Sweden: a review of its character and evolution*. Geological Survey of Finland, Special Paper no. 37, 125 pp.

HÖGDAHL, K. & SJÖSTRÖM, H. 2001. Evidence for 1.82 Ga transpressive shearing in a 1.85 Ga granitoid in central Sweden: implications for the regional evolution. *Precambrian Research* **105**, 37–56.

HOPGOOD, A. M., BOWES, D. R., KOUVO, O. & HALLIDAY, A. D. 1983. U–Pb and Rb–Sr isotopic study of polyphase deformed migmatites in the Svecokarelides, southern Finland. In *Migmatites, Melting and Metamorphism* (eds M. P. Atherton & C. D. Gribble), pp. 80–92. Nantwich: Shiva.

HUHMA, H. 1986. Sm–Nd, U–Pb and Pb–Pb isotopic evidence for the origin of the early Proterozoic Svecokarelian crust in Finland. *Geological Survey of Finland Bulletin* **337**, 48 pp.

KÄHKÖNEN, Y., HUHMA, H. & ARO, K. 1989. U–Pb zircon ages and Rb–Sr whole-rock isotope studies of early Proterozoic volcanic and plutonic rocks near Tampere, southern Finland. *Precambrian Research* **45**, 27–43.

KÄHKÖNEN, Y., LAHTINEN, R. & NIRONEN, M. 1994. Palaeoproterozoic supracrustal belts in southwestern Finland. In *High temperature–low pressure metamorphism and deep crustal structures* (ed. M. Pajunen), pp. 43–7. Meeting of IGCP project 304 'Deep Crustal processes' in Finland, 1994. Geological Survey of Finland Guide no. 37.

KILPELÄINEN, T. 1998. Evolution and 3D modelling of structural and metamorphic patterns of the Palaeoproterozoic crust in the Tampere–Vammala area, southern Finland. *Geological Survey of Finland Bulletin* **397**, 124 pp.

KINNY, P. D., MCNAUGHTON, N. J., FANNING, C. M. & MAAS, R. 1994. 518 Ma sphene (titanite) from the Khan pegmatite, Namibia, southwest Africa: A potential ion-microprobe standard. *Eighth International Conference on Geochronology, Cosmochronology and Isotope Geology Abstracts: Berkeley, US Geological Survey Circular* **1107**, p. 171.

KORJA, A. & HEIKKINEN, P. 1995. Proterozoic extensional tectonics of the central Fennoscandian Shield: results from the Baltic and Bothnian Echoes from the Lithosphere experiment. *Tectonics* **14**, 504–17.

KORSMAN, K., KOISTINEN, T., KOHONEN, J., WENNERSTRÖM, M., EKDAHL, E., HONKAMO, M., IDMAN, H. & PEKKALA, Y. 1997. *Bedrock Map of Finland 1:1,000,000 scale*. Espoo: Geological Survey of Finland.

KORSMAN, K., KORJA, T., PAJUNEN, M., VIRRANSALO, P. & GGT/SVEKA WORKING GROUP. 1999. The GGT/SVEKA transect: Structure and evolution of the continental crust in the Paleoproterozoic Svecofennian orogen in Finland. *International Geology Review* **41**, 287–333.

KROGH, T. E. 1973. A low-contamination method for hydrothermal decomposition of U and Pb for isotopic age determinations. *Geochimica et Cosmochimica Acta* **37**, 485–94.

KROGH, T. E. 1982. Improved accuracy of U–Pb zircon ages by the creation of more concordant systems using an air abrasion technique. *Geochimica et Cosmochimica Acta* **46**, 637–49.

KURHILA, M., VAASJOKI, M., MÄNTTÄRI, I., RÄMÖ, T. & NIRONEN, M. 2005. U–Pb ages and Nd isotope characteristics of the late orogenic, migmatizing microcline granites in southwestern Finland. *Geological Society of Finland Bulletin* **77**, 105–28.

LAHTINEN, R. 1994. Crustal evolution of the Svecofennian and Karelian domains during 2.1–1.79 Ga, with special emphasis on the geochemistry and origin of 1.93–1.91 Ga gneissic tonalities and associated supracrustal rocks in the Rautalampi area, central Finland. *Geological Survey of Finland Bulletin* **378**, 128 pp.

LAHTINEN, R. 1996. Geochemistry of Palaeoproterozoic supracrustal and plutonic rocks in the Tampere–Hämeenlinna area, southern Finland. *Geological Survey of Finland Bulletin* **389**, 113 pp.

LAHTINEN, R. & HUHMA, H. 1997. Isotopic and geochemical constraints on the evolution of the 1.93–1.79 Ga Svecofennian crust and mantle in Finland. *Precambrian Research* **82**, 13–34.

LAHTINEN, R., KORJA, A. & NIRONEN, M. 2005. Paleoproterozoic tectonic evolution. In *Precambrian Geology of Finland – Key to the Evolution of the Fennoscandian Shield* (eds M. Lehtinen, P. A. Nurmi & O. T. Rämö), pp. 481–532. Amsterdam: Elsevier B.V.

LEVIN, T., ENGSTRÖM, J., LINDROOS, A., BALTYBAEV, S. & LEVCHENKOV, O. 2005. Late Svecofennian transpressive deformation in SW Finland – evidence from late-stage D3 structures. *Geologiska Föreningens i Stockholm Förhandlingar (GFF)* **127**, 127–37.

LUDWIG, K. R. 1991. *PbDat 1.21 for MS-DOS: a computer program for IBM-PC compatibles for processing raw Pb–U–Th isotope dataVersion 1.07*. US Geological Survey Open-File Report no. 88–542, 35 pp.

LUDWIG, K. R. 2003. *Isoplot/Ex 3. A geochronological toolkit for Microsoft Excel*. Berkeley Geochronology Center, Special Publication no. 4.

LUUKKONEN, A. 1994. Main geological features, metallogeny and hydrothermal alteration phenomena of certain gold and gold-tin-tungsten prospects in southern Finland. *Geological Survey of Finland Bulletin* **377**, 153 pp.

LUUKKONEN, A., GRÖNHOLM, P. & HANNILA, T. 1992. Eräiden Etelä-Suomen kulta-ja sen seuralaismetalliesiintymien geologiset pääpiirteet. Summary: Main geological features of certain gold and tungsten-tin-gold prospects in southern Finland. *Geological Survey of Finland Report of Investigation* **113**, 1–9.

MATISTO, A. 1978. *Huittisten kartta-alueen kallioperä. Suomen geologinen kartta 1:100 000, kallioperäkartan selitykset 2112 Huittinen* (with English summary: Precambrian rocks of the Huittinen map-sheet area). Espoo: Geological Survey of Finland, 30 pp.

MOURI, H., KORSMAN, K. & HUHMA, H. 1999. Tectono-metamorphic evolution and timing of the melting processes in the Svecofennian tonalite–trondhjemite migmatite belt: an example from Luopoinen, Tampere area, southern Finland. *Geological Survey of Finland Bulletin* **71**, 31–56.

MOURI, H., VÄISÄNEN, M., HUHMA, H. & KORSMAN, K. 2005. Sm–Nd garnet and U–Pb monazite datig of high-grade metamorphism and crustal melting in the West Uusimaa area, southern Finland. *Geologiska Föreningens i Stockholm Förhandlingar (GFF)* **127**, 123–8.

NIIRANEN, T., POUTIAINEN, M. & MÄNTTÄRI, I. 2007. Geology, geochemistry, fluid inclusion characteristics, and U–Pb age studies from iron oxide Cu–Au deposits in the Kolari region, northern Finland. *Ore Geology Reviews* **30**, 75–105.

NIRONEN, M. 1999. Structural and magmatic evolution in the Loimaa area, southwestern Finland. *Geological Society of Finland Bulletin* **71**, 57–71.

NIRONEN, M. & KÄHKÖNEN, Y. (eds) 1994. *Geochemistry of Proterozoic Supracrustal Rocks in Finland*. Geological Survey of Finland Special Paper no. 19, 184 pp.

PAJUNEN, M., AIRO, M. L., ELMINEN, T., MÄNTTÄRI, I., NIEMELÄ, R., VAARMA, M., WASENIUS, P. & WENNERSTRÖM, M. 2008. Tectonic evolution of Svecofennian crust in southern Finland. *Geological Survey of Finland Special Publication* **47**, 15–184.

PATCHETT, J. & KOUVO, O. 1986. Origin of continental crust of 1.9–1.7 Ga age: Nd isotopes and U–Pb zircon ages in the Svecokarelian terrain of South Finland. *Contributions to Mineralogy and Petrology* **92**, 1–12.

PATISON, N. L. 2007. Structural controls on GOLD mineralisation in the Central Lapland Greenstone Belt. In *Gold in the Central Lapland Greenstone Belt, Finland* (ed. V. J. Ojala), pp. 107–22. Geological Survey of Finland, Special Paper no. 44.

PIDGEON, R. T., BOSCH, D. & BRUGUIER, O. 1996. Inherited zircon and titanite U–Pb systems in an Archaean syenite from southwestern Australia: implications for U–Pb stability of titanite. *Earth and Planetary Science Letters* **141**, 187–98.

PUUSTINEN, K., SALTIKOFF, B. & TONTTI, M. 1995. Distribution and metallogenic types of nickel deposits in Finland. *Geological Survey of Finland Report of Investigation* **132**, 38 pp.

RÄMÖ, O. T., VAASJOKI, M., MÄNTTÄRI, I., ELLIOTT, B. A. & NIRONEN, M. 2001. Petrogenesis of the post-kinematic magmatism of the Central Finland Granitoid Complex I: radiogenic isotope constraints and implications for crustal evolution. *Journal of Petrology* **42**, 1971–93.

ROMER, R. L. & SMEDS, S. A. 1997. U–Pb columbite chronology of post-kinematic Palaeoproterozoic pegmatites in Sweden. *Precambrian Research* **82**, 85–99.

RUTLAND, R. W. R., WILLIAMS, I. S. & KORSMAN, K. 2004. Pre-1.91 Ga deformation and metamorphism in the Palaeoproterozoic Vammala Migmatite Belt, southern Finland, and implications for Svecofennian tectonics. *Geological Society of Finland Bulletin* **76**, 93–140.

SAALMANN, K. 2007. Structural control on gold mineralization in the Satulinmäki and Riukka prospects, Häme schist belt, southern Finland. *Geological Society of Finland Bulletin* **79**, 69–93.

SAALMANN, K., MÄNTTÄRI, I., PELTONEN, P. & WHITEHOUSE, M. J. 2008. Timing of orogenic gold mineralization in southern Finland and its relationship to the Palaeoproterozoic Svecofennian tectonic evolution. *33rd International Geological Congress, 6–14 August 2008, Oslo, Norway*. Abstract CD-ROM, 1 p.

SALTIKOFF, B., PUUSTINEN, K. & TONTTI, M. 2006. *Metallogenic zones and metallic mineral deposits in Finland. Explanation to the Metallogenic Map of Finland*. Geological Survey of Finland Special Paper no. 35, 66 pp.

SCHÄRER, U., ZHANG, L. S. & TAPPONNIER, P. 1994. Duration of strike-slip movements in large shear zones: the Red River belt, China. *Earth and Planetary Science Letters* **126**, 379–97.

SCOTT, D. J. & ST-ONGE, M. R. 1995. Constraints on Pb closure temperature in titanite based on rocks from the Ungava Orogen, Canada; implications for U–Pb geochronology and P–T–t path determinations. *Geology* **23**, 1123–6.

SKRIDLAITE, G. & MOTUZA, G. 2001. Precambrian domains in Lithuania: evidence of terrane tectonics. *Tectonophysics* **339**, 113–33.

SKYTTÄ, P. 2007. *Svecofennian crustal evolution in the Uusimaa belt area, SW Finland*. Espoo: Geological Survey of Finland, 17 pp.

STACEY, J. S. & KRAMERS, J. D. 1975. Approximation of terrestrial lead isotope evolution by a two-stage model. *Earth and Planetary Science Letters* **26**, 207–21.

TORVELA, T., MÄNTTÄRI, I. & HERMANSSON, T. 2008. Timing of deformation phases within the South Finland shear zone, SW Finland. *Precambrian Research* **160**, 277–98.

VÄISÄNEN, M. & HÖLTTÄ, P. 1999. Structural and metamorphic evolution of the Turku migmatite complex, southwestern Finland. *Geological Society of Finland Bulletin* **71**, 177–218.

VÄISÄNEN, M., MÄNTTÄRI, I. & HÖLTTÄ, P. 2002. Svecofennian magmatic and metamorphic evolution in southwestern Finland as revealed by U–Pb zircon SIMS geochronology. *Precambrian Research* **116**, 111–27.

VÄISÄNEN, M. & SKYTTÄ, P. 2007. Late Svecofennian shear zones in southwestern Finland. *Geologiska Föreningens i Stockholm Förhandlingar (GFF)* **129**, 55–64.

VALBRACHT, P. J., OEN, I. S. & BEUNK, F. F. 1994. Sm–Nd isotope systematics of 1.9–1.8 Ga granites from western Bergslagn, Sweden: inferences on a 2.1–2.0 Ga crustal precursor. *Chemical Geology* **112**, 21–37.

VERTS, L. A., CHAMBERLAIN, K. R. & FROST, C. D. 1996. U–Pb sphene dating of metamorphism: the importance of sphene growth in the contact aureole of the Red Mountain Pluton, Laramie Mountains, Wyoming. *Contributions to Mineralogy and Petrology* **125**, 186–99.

VUORI, S., KÄRKKÄINEN, N., HUHTA, P. & VALJUS, T. 2005. Ritakallio gold prospect, Huittinen, SW Finland. *Geological Survey of Finland Report of Investigation* **CM06/2112/2005/1/10**, 53 pp.

WEIHED, P., BILLSTRÖM, K., PERSSON, P.-O. & BERGMAN WEIHED, J. 2002. Relationship between 1.90–1.85 Ga accretionary processes and 1.82–1.80 Ga oblique subduction at the Karelian craton margin, Fennoscandian Shield. *Geologiska Föreningens i Stockholm Förhandlingar (GFF)* **124**, 163–80.

WHITEHOUSE, M. J. & KAMBER, B. S. 2005. Assigning Dates to Thin Gneissic Veins in High-Grade Metamorphic Terranes: A Cautionary Tale from Akilia, Southwest Greenland. *Journal of Petrology* **46**, 291–318.

WHITEHOUSE, M. J., KAMBER, B. & MOORBATH, S. 1999. Age significance of U–Th–Pb zircon data from early Archaean rocks of west Greenland – a reassessment based on combined ion-microprobe and imaging studies. *Chemical Geology* **160**, 201–24.

WIEDENBECK, M., ALLÉ, P., CORFU, F., GRIFFIN, W. L., MEIER, M., OBERLI, F., VON QUADT, A., RODDICK, J. C. & SPIEGELN, W. 1995. Three natural zircon standards for U–Th–Pb, Lu–Hf, trace element and REE analysis. *Geostandards Newsletter* **19**, 1–23.

WISZNIEWSKA, J., KRZEMINSKA, E. & DÖRR, W. 2007. Evidence of arc-related Svecofennian magmatic activity in the southwestern margin of the East European Craton in Poland. *Gondwana Research* **12**, 268–78.